Distribution Agreement

In presenting this thesis or dissertation as a partial fulfillment of the requirements for an advanced degree from Emory University, I hereby grant to Emory University and its agents the non-exclusive license to archive, make accessible, and display my thesis or dissertation in whole or in part in all forms of media, now or hereafter known, including display on the world wide web. I understand that I may select some access restrictions as part of the online submission of this thesis or dissertation. I retain all ownership rights to the copyright of the thesis or dissertation. I also retain the right to use in future works (such as articles or books) all or part of this thesis or dissertation.

Signature:

_____ _____

Xinxian Shao Date

EXPLORING BACTERIAL INFECTIONS: THEORETICAL AND EXPERIMENTAL STUDIES OF THE BACTERIAL POPULATION DYNAMICS AND ANTIBIOTIC TREATMENT

By

Xinxian Shao
Doctor of Philosophy
Physics

_____
Ilya Nemenman, Ph.D., Advisor

_____
Bruce Levin, Ph.D., Co-advisor

_____
Eric Weeks, Ph.D., Committee Member

_____
Stefan Boettcher, Ph.D., Committee Member

_____
Minsu Kim, Ph.D., Committee Member

_____
Andrew Mugler, Ph.D., Committee Member

Accepted:

_____
Lisa A. Tedesco, Ph.D.
Dean of the James T. Laney School of Graduate Studies

_____
Date

EXPLORING BACTERIAL INFECTIONS: THEORETICAL AND EXPERIMENTAL STUDIES OF THE BACTERIAL POPULATION DYNAMICS AND ANTIBIOTIC TREATMENT

By

Xinxian Shao
B. Sc., University of Science and Technology of China, 2010

Advisor: Ilya Nemenman, Ph. D.
Co-advisor: Bruce Levin, Ph. D.

An abstract of
A dissertation submitted to the Faculty of the
James T. Laney School of Graduate Studies of Emory University
in partial fulfillment of the requirements for the degree of
Doctor of Philosophy
in Physics
2016

Abstract

EXPLORING BACTERIAL INFECTIONS: THEORETICAL AND EXPERIMENTAL STUDIES OF THE BACTERIAL POPULATION DYNAMICS AND ANTIBIOTIC TREATMENT

By Xinxian Shao

ABSTRACT

Exploring Bacterial Infections Theoretical and Experimental:
Studies of the Bacterial Population Dynamics and
Antibiotic Treatment

Xinxian Shao

Bacterial infections are very common in human society. Thus extensive research has been conducted to reveal the molecular mechanisms of the pathogenesis and to evaluate the antibiotics' efficacy against bacteria. Little is known, however, about the population dynamics of bacterial populations and their interactions with the host's immune system. In this dissertation, a stochatic model is developed featuring stochastic phenotypic switching of bacterial individuals to explain the single−variant bottleneck discovered in multi strain bacterial infections. I explored early events in a bacterial infection establishment using classical experiments of Moxon and Murphy on neonatal rats. I showed that the minimal model and its simple variants do not work. I proposed modifications to the model that could explain the data quantitatively. The bacterial infections are also commonly established in physical structures, as biofilms or 3-d colonies. In contrast, most research on antibiotic treatment of bacterial infections has been conducted in well-mixed liquid cultures. I explored the efficacy of antibiotics to treat such bacterial colonies, a broadly applicable method is designed and evaluated where discrete bacterial colonies on 2-d surfaces were exposed to antibiotics. I discuss possible explanations and hypotheses for the experimental results. To verify these hypotheses, we investigated the dynamics of bacterial population as 3-d colonies. We showed that a minimal mathematical model of bacterial colony growth in 3-d was able to account for the experimentally observed presence of a diffusion-limited regime. The model further revealed highly loose packing of the cells in 3-d colonies and smaller cell sizes in colonies than plancktonic cells in corresponding liquid culture. Further experimental tests of the model predictions have revealed that the ratio of the cell size in liquid culture to that in colony cultures

was consistent with the model prediction, that the dead cells emerged randomly in a colony, and that the cells packed heterogeneously in the outer part of a colony, possibly explaining the loose packing.

EXPLORING BACTERIAL INFECTIONS: THEORETICAL AND EXPERIMENTAL STUDIES OF THE BACTERIAL POPULATION DYNAMICS AND ANTIBIOTIC TREATMENT

By

Xinxian Shao
B. Sc., University of Science and Technology of China, 2010

Advisor: Ilya Nemenman, Ph. D.
Co-advisor: Bruce Levin, Ph. D.

A dissertation submitted to the Faculty of the
James T. Laney School of Graduate Studies of Emory University
in partial fulfillment of the requirements for the degree of
Doctor of Philosophy
in Physics
2016

To

My beloved parents,

My husband Heng,

and

My dearest Muffin

ACKNOWLEDGEMENTS

I thank my advisor Dr. Ilya Nemenman, for always being supportive and inspiring. I learned so much from his enthusiasm in science and meticulous scholarship.

I thank Dr. Bruce Levin. Thank you for giving me the opportunity to work with you. Our lab is always full of energy and laughter.

I thank my committee members Dr. Eric Weeks, Dr. Stefan Boettcher, Dr. Minsu Kim, and Dr. Andrew Mugler. Thank you for your support and encouragement.

Many thanks to my friends and colleges at Emory, especially Baohua Zhou, George Leung, Catalina Rivera, Emrah Simsek, Ms. Nina Walker, Ingrid McCall, Mr. Jason Boss and many others, for their companionship and help during my graduate life.

TABLE OF CONTENTS

LIST OF TABLES

LIST OF FIGURES

CHAPTER I

INTRODUCTION

Infectious diseases have affected human populations throughout the entire history of our species. Before advances in the underlying science of health and medicine, infectious diseases were often epidemic and developed into plagues with high mortality rates. *Yersinia pestis*, the causative agent of the *Black Death*, struck the European population in the 14^{th} century, and killed nearly 24 million of the European population [1, 2].

People has been searching for cures for these illnesses and the means of stopping the spread of the infections since the dawn of time. Theories were developed, from miasma to germ theory, but none of those could be verified until the invention of microscopes by Leeuwenhoek. His discovery of microbes [2] significantly pushed forward the scientific understanding of infectious diseases [3, 4]. Regarded as one of main founders of bacteriology, Louis Pasteur (1822–1895) proposed the principles of microbial fermentation in 1857 [5], invented pasteurization and experimentally confirmed the germ theory of infectious diseases. In the subsequent decades, numerous scientists studying infectious diseases conducted extensive experimental research, leading to the identification of many causative microorganisms of specific infectious diseases, as well as proposing better treatments for some of the diseases. From the concept of "magic bullet" by Paul Ehrlich (1854–1915), to the vaccine against anthrax by Toussaint (1847–1890), and the discovery of penicillin by Alexander Fleming (1881–1955), the mortality of infectious diseases has decreased dramatically, and the human life span around the world has lengthened because of the development in microbiology and the disciplines derived from it, such as immunology, virology and epidemiology [4, 6] .

The concept of immunity, playing an important role in the development of vaccines, dates back at least to Greece from the 5th century BC when Thucydides discribed that the individuals who had recovered from a disease became "immune" to this disease [7]. In 1882, Elie Metchnikoff discovered phagocytes, a major contribution to the establishment of the mechanism of innate immunity [8]. By that time, we knew that the immune system in our body protects us from infections even if we are exposed to pathogenic microorganisms all the time. Little was known, however, about the dynamics of how bacterial populations survive from the immune response, colonize the host, invade tissues and cells, and thereby cause diseases.

To understand the within-host dynamics of bacterial infections, a hypothesis of independent action was proposed by Druett in 1952 [9], assuming that each individual bacterial cell has an independent probability to colonize the host. Meynell and Stocker verified the hypothesis of independent action experimentally [10] against the hypothesis of synergistic action or cooperative action. Furthermore, Meynell applied the hypothesis to *Salmonella typhimurium* infections in mice, discovering the single−variant bottleneck, a phenomenon that only one variant of *Salmonella typhimurium* appeared in fatally infected mice when they were inoculated with a mixture of multiple equally virulent variants of this bacteria. He proposed that the infections were possibly initiated by only a single organism. Similar observations were reported in experimental studies of host-virus interactions [11, 12, 13, 14, 15]. Two decades later, in a series of experimental studies of *Haemophilus influenzae* pathogenesis, Moxon and Murphy again observed the single−variant bottleneck [16, 17]. In their experiments, when inoculated intranasally with a mixture of equally virulent strains of *Haemophilus influenzae* type b(*Hib*), neonatal rats developed a bacteremic infection that often was dominated by only one random strain of two equally pathogenic competing strains. While Moxon and Murphy discussed the applicability of the hypothesis of independent action to their experiments, several hypotheses and experiments were reported

trying to explain this phenomenon mechanistically. These included host susceptibility, the emergence of bacterial mutants (known as within-host evolution) [18, 19, 20]. Unfortunately, none of these were able to quantitatively explain the experimental data of the single−variant bottleneck. In Chapter 2 of this dissertation, I present a mathematical model for a common hypothesis that explains the single−variant bottleneck as stochastic phenotypic switching in individual bacterial cells. This hypothesis predicts that the first successful switching cell in one strain interacts with the host immune response to "shut the door" in front of the other strain. To mimic the experiments described in [16], I implemented this model as a set of mixed stochastic and deterministic differential equations. I conclude that this model, as well as its simple variants, cannot explain the experimental data reported in [16], and namely the observed weak dependence of the rate of infections on the inoculum size. I propose modifications to the model that could explain the data, and discuss possible biological and cellular mechanisms that could lead to such modifications.

Even though people have made spectacular progress in the fields of microbiology, virology, immunology, as well as epidemiology and public health, the threats of infectious diseases have not been eliminated. On the one hand, resistant strains of bacteria emerged not long after the antibiotics became widely available. These resistant strains are often more virulent than the wild type strains [21, 22, 23]. On the other hand, some conditions have turned out to be very hard to treat, such as bacterial infections that develop as spatial structures, including biofilms and 3-d colonies [24, 25, 26]. Even though we have been exploring the micriobial world under microscopes for centuries, it was not until the 1970s that bacteria in biofilms and colonies were considered as an important component of the research of microbiology [27]. They are now increasingly appreciated in the studies of chronic diseases [28]. According to CDC (the Centers for Disease Control and Prevention), over two thirds

of bacterial infections clinically treated in developed countries involve bacterial colonizations in the form of colonies, microcolonies or biofilms [24, 25, 29]. *Staphylococcus aureus* is one of the most common species that can be seen in these infections [26]. One way to fight against bacterial colonies and biofilms is to prevent the growth of these populations in the first place. Antimicrobial agents or nanomaterial coatings, such as vancomycin-modified titanium alloys, antiseptics chlorhexidin and silver sulfadiazine, can be applied to the surface of biomaterials and devices to impair the aggregation and proliferation of bacteria [30, 31, 32]. Otherwise, the most effective treatment of bacterial infections involving colonies or biofilms are considered to be their mechanical destruction, which, however, cannot be performed in most cases [33]. When mechanical destruction is impossible, antibiotics remain the standard option against bacterial infections. Unfortunately, it is well known that bacterial colonies and biofilms are highly refractory to a broad selection of antibiotics [25, 33, 34]. In Chapter 3, I present a novel method to quantitatively evaluate (1) the *in vitro* efficacy of antibiotics to treat bacteria growing as discrete colonies on surfaces and (2) the contribution of the colony structure to the antibiotic susceptibility of bacteria. Using this method, I explored the relative efficacy of six bactericidal and three bacteriostatic antibiotics to inhibit the growth and kill *Staphylococcus aureus* colonies of different sizes, densities, and ages. I discuss possible reasons to the observed failure of treatments based on experimental results from previous studies. The wide variation of the efficacies of these antibiotics raises many new questions regarding the population dynamics and the physical structure of bacterial colonies. These questions, for now, remain unanswered.

As a step towards answering these questions, it is crucial to build a theoretical model that can provide quantitative predictions and can be falsified experimentally. There have been many mathematical models developed for bacterial population on

surfaces. In 1998, Kreft *et al.* designed a simulator, named BacSim, for two dimensional bacterial growth as a biofilm [35]. This was the first simulator that was implemented based on modeling growth of individual bacterial cells instead of cellular automata models [36, 37, 38, 39]. In the following decades, more mathematical models have been developed for bacterial growth on 2-d surfaces forming complex two or three dimensional morphologies [40, 41, 42, 43, 44, 45, 46, 47, 48]. These new models, mostly inspired by the observations from advanced experimental systems, all feature large numbers of parameters to describe highly complex reactions and mechanisms and produce highly detailed predictions of the geometry and physiology of the considered bacterial population. However, few of these predictions have be quantitatively verified by or compared to experimental data. In Chapter 4, I present a minimal model for bacterial populations growing as colonies in three dimensions (3-d) and designed an experimental system of quantitatively-controlled 3-d colony growth of *Escherichia coli*. By extending the classic Monod model of resource-limited population growth to allow for spatial heterogeneity in the bacterial access to nutrients, our 3-d model of colonies describes the dynamics of bacteria consuming diffusing nutrients in their vicinity. By following the changes in density of *E. coli* in liquid and as colonies embedded in glucose-limited soft agar, I evaluate the fit of this model to experimental data. The growth dynamics and the physical structure of 3-d colonies that are revealed in this combined theoretical-experimental study have different characters from that of bacterial populations developed on 2-d surfaces. Our model provides a baseline description of bacterial growth in 3-d, deviations from which can be used to identify phenotypic heterogeneities and inter-cellular interactions that further contribute to the structure of bacterial communities.

Some predictions of the model are surprising, opening venues for additional research. It has been reported in several experimental studies that bacterial cells regulate the cell size according to their growth rates [49, 50, 51, 52, 53]. However, no

corresponding data have been reported for bacterial colonies. Our experiment of *E. coli* growth revealed that the yield of bacteria from the same amount of nutrients was higher in colonies than in liquid cultures, paralleling the observations in Simonsen's experiment [54]. Our model also predicts heterogeneous growth rates in a 3-d colony. Based on these results of previous studies and my research, I hypothesize that the cell size in colonies is smaller than that in liquid cultures. Secondly, according to the nutrient distribution described by the model, the starvation of bacterial cells would start from the center of a colony, thereby the cells in the center should be the first ones that die. This seemingly reasonable prediction also needs experimental verification. Thirdly and surprisingly, the packing density of bacterial cells in a 3-d colony is revealed to be relatively loose by two independent methods in Chapter 4, comparing to that of 2-d colonies or biofilms reported in previous studies [55, 56]. In order to verify the predictions of our model and answer these questions raised from it, I present single-cell experiments also in Chapter 4, involving confocal microscopy and fluorescence tagging on bacterial components. The experimental results confirmed the hypothesis of cell size in 3-d colonies, demonstrated the spatial distribution of dead cells, and illustrated loose cell packing in 3-d colonies. This study of 3-d colony growth of *Escherichia coli* reveals valuable features of the bacterial population dynamics as colonies, provides more possible insights into treatments against bacterial infections in physically structured morphologies.

Overall, in this Dissertation, I present a comprehensive study of the bacterial infections and population dynamics that involves both experimental work and theoretical work. In Chapter 5, I briefly summarize the general conclusions of the investigations presented in this dissertation and discuss their contribution to science and research. Based on the results and discoveries of these investigations, I propose additional questions and potential future directions.

CHAPTER II

SINGLE VARIANT BOTTLENECK IN THE EARLY DYNAMICS OF *H. INFLUENZAE* BACTEREMIA IN NEONATAL RATS QUESTIONS THE THEORY OF INDEPENDENT ACTION

(This chapter is based on "Shao, X., Levin, B., & Nemenman, I. (2016). Single variant bottleneck in the early dynamics of *H. influenzae* bacteremia in neonatal rats questions the theory of independent action *arXiv preprint arXiv:*".)

2.1 Introduction

Before the *Hib* (*Haemophilus influenzae* type b) conjugate vaccine was developed and taken into routine use in U.S., *H. influenzae* was the leading cause of bacterial meningitis in children under age 5 [57]. At the same time, bacterial meningitis had high mortality and serious residua, including deafness, blindness and mental retardation. Even today, the lack of vaccines in the developing countries and the genetic diversity among bacterial strains still result in the mortality rate from *H. influenzae* infections in the developing world reaching 14.3% [57].

The high impact of the disease has led Moxon and Murphy to develop its neonatal rat experimental model in 1974 to study the pathogenesis of meningitis caused by *Hib* [16, 17]. It was revealed that the infection involved three main stages: nasopharyngeal colonization, bacteremia, and central nervous system (CNS) invasion. By intranasally inoculating the neonatal rats with two equally virulent variants of *H. influenzae* and tracking development of bacteremia and meningitis, they found that, while five minutes after inoculation *both variants* were found in the blood, nearly

70% of rats ended up with a single bacterial variant in the blood (Fig. 2.1) and cerebrospinal fluid cultures taken at least 24 hrs after inoculation, and both variants occurred in different subjects with nearly equal frequency [16]. The phenomenon that the primary infections (nasal colonization and early blood flora for *Hib*) are diverse, while mature infections (blood after > 10 hrs for *Hib*) seem to contain just one strain is known as the *single-variant bottleneck*. The bottleneck is not unique to *Hib*. In fact, it was discovered first by Meynell in *Salmonella typhimurium* infections in mice [10]. And similar observations have been reported in experimental studies of other host-bacterium [58, 59, 60] and host-virus [11, 12, 13, 14, 15, 61, 62] interactions. Conceptual model of the early infection must be able to explain the single-variant bottleneck, and also the fact that, in the wild, only minority of hosts (e. g., children under 5 [16, 57]) end up with infections even for the most virulent strains of this bacteria. For this, three classes of possible explanations have been proposed: stochasticity resulting from *independent action* of bacteria [10, 63, 64, 65, 66], host susceptibility, and the emergence of bacterial mutants (known as within-host evolution) [18, 19, 20]. The original hypothesis of independent action was proposed by Druett in 1952 [9]. It assumed that each individual bacterial cell has an independent probability to colonize the host, and that an infection can start from a single random bacterium, hence explaining the bottleneck. Meynell and Stocker later verified the hypothesis of independent action experimentally [10] against the hypothesis of synergistic or cooperative action. However, in its simple form, independent action could not explain why a variant present in the blood five minutes post-inoculation would disappear hours later. Host susceptibility could only explain the high infection rate in young children over adults, but also not the observation of the presence of both variants in the bloodstream at the very early post-inoculation stage [16]. Finally, to test the within-host evolution hypothesis, Margolis and Levin performed

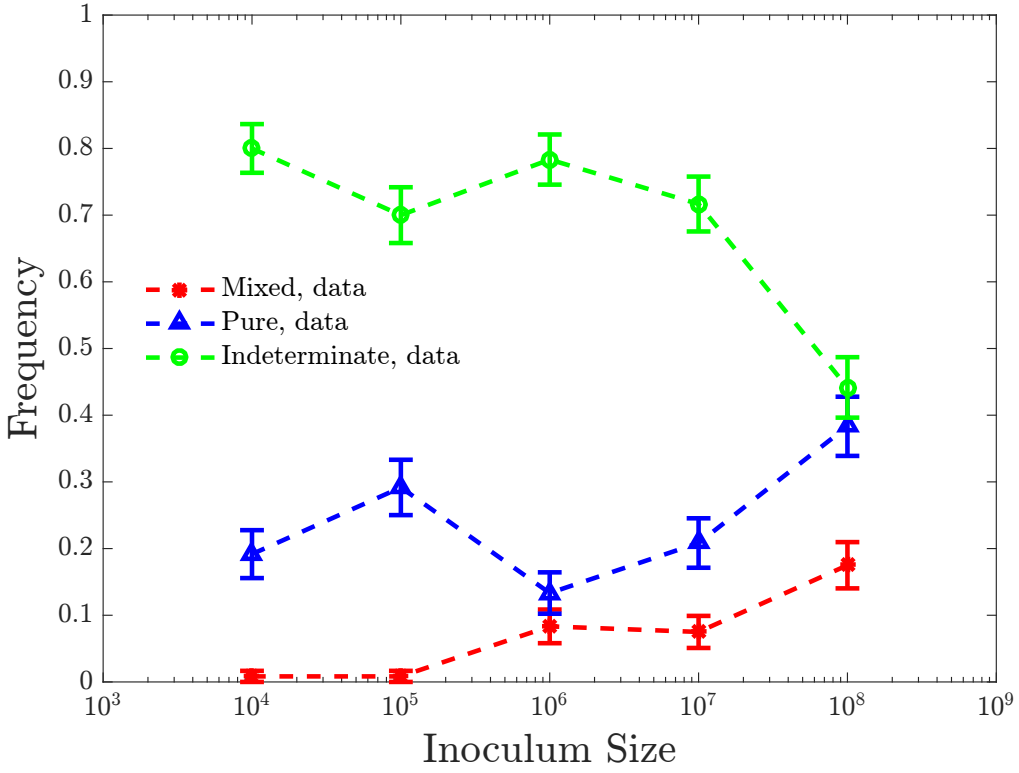

Figure 2.1: **Moxon and Murphy's experimental data.** Replotted from [16]. 120 neonatal rats were infected at each inoculum size, which ranged from 10^4 to 10^8 bacteria, equally mixed from streptomycine susceptible strain, Sm^S, and streptomycine resistant strain, Sm^R. Blood of the rats was then harvested and cultured. All cultures that produced both Str^S and Str^R colonies were called *mixed* infections. All cultures that produced 8 or more colonies of one strain and none of the other were called *pure* infections (there was no statistically significant difference in the abundance of pure Sm^S or pure Sm^R cultures). Cultures that produced no colonies, or produced colonies of one strain only, but fewer than 8 of those, were called indeterminate. Most infections ended up as pure (single-variant) infections 54 hours post-inoculum. Samples taken within 5 and 30 minutes post-inoculum were mixed (data not show on the plot) shown on the plot, see Ref. [16]). Error bars denote the usual square-root counting errors. Over four orders of magnitude in the inoculum size, preponderance of indeterminate infections declined somewhat, from $\sim$80% to $\sim$40%. Over the same range of the inoculum, mixed infections increased from $<$1% to $\sim$20%.

additional *H. influenzae* experiments with neonatal rats. They compared the invasiveness and the re-colonization potential of the variant surviving in the bloodstream and the remaining variant staying in nasopharynx [20]. In most trials, they observed no advantage of the isolates from infected hosts over the other wild type variant. This ruled out the hypothesis of within-host evolution as a dominant explanation for the single-variant bottleneck.

However, the last decades have shown that bacteria can switch epigenetically among multiple phenotypic states [63, 65, 67, 68, 69, 70, 71]. Such random switching into a faster growing or more virulent state by a single bacterium of one strain can lead to a faster growth of the strain in the blood. And yet the strain will not be genetically favored to win a re-competition with the other. At the same time, the host immune system, activated by the infection, will fight both strains, clearing off the slower growing, non-switched strain from the blood. In other words, the first successfully switching cell in one strain will interact with the host immune response to 'shut the door' in front of the other strain. This would explain the single-variant bottleneck.

This stochastic switching mechanism together with the immune response has been mentioned frequently as a possible explanation for the bottleneck phenomenon in various presentations and discussions, though, surprisingly, we have been unable to find its detailed analysis in the literature. We call this hypothesis the *colloquial hypothesis* in the rest of this work. Our goal here is to analyze the colloquial hypothesis quantitatively and to verify if it can rescue the theory of independent action as the explanation of the single-variant bottleneck in early bacteremia.

In this chapter, we will develop a mathematical model of the colloquial hypothesis applied to the early stages of *Hib* bacteremia inoculated with two variants of equally virulent bacteria. We will show that the model, as well as its simple extensions, cannot quantitatively explain the experimental data [16, 19, 20, 72], and namely the observed

weak dependence of the rate of infections on the inoculum size. We will argue that, to provide even a semi-quantitative fit to the data, we must assume that various rate parameters describing infection scale *sublinearly* with the inoculum size, so that the probability per bacterium to start an infection decreases when other bacteria are present. This means further evidence for abandoning the theory of independent action.

2.2 Hypothesis and Model

Inspired by demonstration of ubiquitous phenotypic switching in bacteria [65, 68, 69, 70, 71, 73, 74, 75], we propose that each individual bacterial cell has two phenotypes relevant for the early infection. The first is the "crossing" phenotype (C), which allows bacteria to cross the physical barrier between the nasopharynx and blood, but does not exhibit strong growth in the bloodstream [76, 77, 78]. The second is the "growing" phenotype (G), with cells that grow fast in the bloodstream, but cannot cross into the bloodstream. After a bacterium crosses into the blood stream, it can switch to the G state, but the switching C→G is stochastic and rare. In this work, we are not concerned with the mechanisms underlying the existence of these two states, and of switching between them, but only focus on consequences of the switching.

Once bacterial cells enter the bloodstream, immune response is activated. To model the immune response in the early stages of bacteremia, we assume that neonatal rats only have innate immunity, which is non-specific and responds as soon as the bacterial cells emerge in the blood [57, 16, 18, 79]. In other words, there is no clonal expansion, and instead there is a finite reservoir of immune cells that can be recruited to the infection site linearly until the reservoir is depleted [79].

These assumptions are represented in the following ordinary differential equations (ODEs) describing the growth of bacterial cells of variant A and the immune cell

recruitment:

$$\frac{dA_C}{dt} = g_C A_C \left(1 - \frac{N_{\text{total}}}{N_0}\right) - \gamma_C I A_C - d A_C + j, \tag{2.1}$$

$$\frac{dA_G}{dt} = g_G A_G \left(1 - \frac{N_{\text{total}}}{N_0}\right) - \gamma_G I A_G - d A_G, \tag{2.2}$$

$$\frac{dI}{dt} = r_C (I_0 - I)(A_C + B_C) + r_G (I_0 - I)(A_G + B_G) - d_I I. \tag{2.3}$$

The growth of the bacterial strain B is described by equations similar to Eqs. (2.1, 2.2), with indices A replaced by B.

In the equations describing bacterial population dynamics, Eqs. (2.1, 2.2), g_C and g_G are the growth rates of the crossing and the growing phenotypes, respectively (same for variants A and B since both variants are equally virulent [16, 20]). For simplicity, in what follows we set $g_C = 0$. N_{total} is the total number of bacteria in the blood, $N_{\text{total}} \equiv A_C + A_G + B_C + B_G$. N_0 is the carrying capacity, the maximum of the bacterial population in the bloodstream, so that $N_0 \geq N_{\text{total}}$. γ_C and γ_G are the bacterial death rates due to the elimination by the immune cells, and d is the natural cell death. Finally, j is the flux of the crossing phenotype cells from the nasopharynx to the bloodstream per unit time. To satisfy the hypothesis of independent action, it is assumed to be linearly proportional to the inoculum size S, so that $j = \alpha_j S$, where α_j is some constant.

Equation (2.3) describes the immune cells recruitment. Here r_C and r_G are the recruitment rates due to effects of the bacterial phenotypes [79]. I_0 is the total number of available innate immune cells in the host. d_I is the death rate, or deactivation rate of immune cells. Parameters in Eq. (2.3) are determined up to a scale. Thus we set $I_0 = 1$, which redefines the scale of I and also renormalizes γ_C and γ_G in Eqs. (2.1, 2.2). To simplify the model, we set $\gamma_C = \gamma_G = \gamma$, and $r_C = r_G = r$.

To finish specifying the model, we assume for now that the switching from C to G is a single step stochastic transition at a low per-bacterium rate ρ. Since the switching is single-step, the waiting time to the switch is exponentially distributed for each cell.

Further, if the independent action hypothesis is valid, then for A_C bacteria in the crossing phenotype, the probability of having k individuals of type A switching to the growing state per time Δt is given by the Poisson distribution:

$$P(k|A_C) = \frac{(\rho A_C \Delta t)^k e^{-\rho A_C \Delta t}}{k!}. \tag{2.4}$$

A similar distribution determines the switching probability for the B strain. We do not consider switching back from the G to the C state.

We simulate the model using the Euler method to solve its ODEs, Eqs. (2.1, 2.2, 2.3) and their equivalents for the B strain. Further, at every time step, we generate a random number of switching individuals using Eq. (2.4) for the A and the B strain. If the number of cells in any strain / phenotypic state combination falls below one, we set it to zero to account for the discreteness of the bacteria. While this combined stochastic-deterministic simulation scheme is certainly not the most accurate, we feel that it offers the precision necessary for our analysis. It certainly is capable of discovering the salient qualitative features of the models that we investigate.

2.3 Results

2.3.1 The colloquial model

We illustrate a possible dynamics of the colloquial model in Fig. 2.2 for the first 60 hours post-inoculum in an individual rat with a certain set of model parameters. In this case, a cell of strain B switched to the growing phenotype first at $t \approx 11$ hrs. Then the rapid growth of B_G accelerated the recruitment of immune cells. In their turn, the immune cells wiped the population of the non-switched strain A, transforming the infection into the pure B infection about 30 h post-inoculation. Therefore, even though cells act independently, they interact through the immune response, and the first variant to have a switcher wins the competition. This example illustrates that the colloquial hypothesis may have a potential to explain the single-variant bottleneck in the early stages of bacteremia.

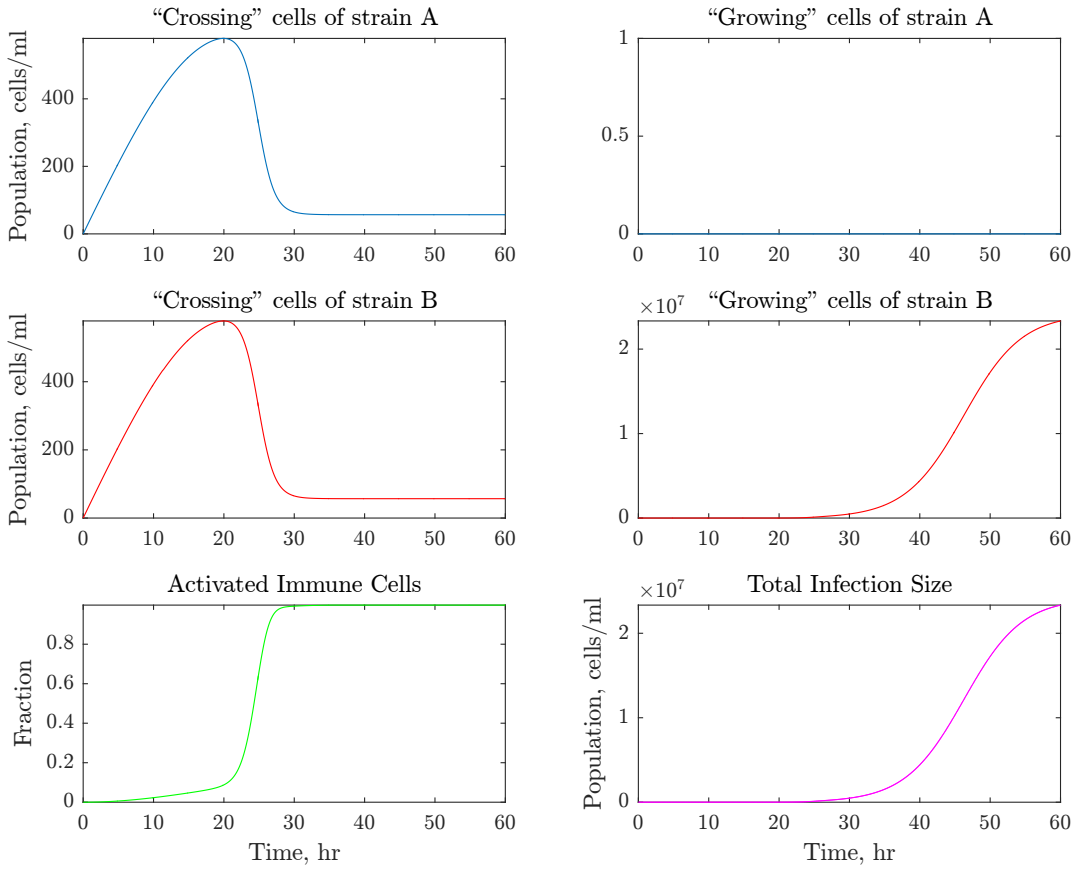

Figure 2.2: **Simulation of early bacteremia resulting in a pure infection in an individual rat.** Simulations were done with the following parameters: inoculum size $S = 10^5$; organisms; switching rate : $\rho = 4.5 \cdot 10^{-5}$ h^{-1}; growth rates $g_C = 0$, $g_G = 1$ h^{-1}; immune recruitment rates $r_C = r_G = 6.1 \cdot 10^{-6}$ h^{-1}; rate at which immune cells kill bacteria $\gamma_C = \gamma_G = 0.75$ h^{-1}; carrying capacity of the blood $N_0 = 10^8$ cells; flux from the nasopharynx to blood $\alpha_j = 4.3 \cdot 10^{-4}$ cells/h; natural death rate of bacteria and immune cells $d = 0.01$ h^{-1} and $d_I = 0.02$ h^{-1}. In this realization, variant strain B has the first switching from C to G at about 11 hours and establishes bacteremia. The panels show the population size of the crossing and the growing phenotypes of A and B strains, the fraction of the immune response activated, and the total infection size. Notice that the vertical axes in different panels have different scalings.

To test the suitability of the colloquial model quantitatively, we calculate and maximize its likelihood given the observed experimental data. As in the Moxon and Murphy experiment, we assume the multinomial structure of the data with three possible outcomes: pure infection, mixed infection, and indeterminate infection. Recall that Moxon and Murphy plated blood samples from their rats and counted the number of colonies of each strain that grew as a result. They defined any culture with colonies of both strains (even if one of the strains had as few as one colony) as a mixed infection. A pure infection was defined more stringently, so that there had to be at least eight colonies of one strain and none of the other to qualify. All other cases were deemed indeterminate. In our simulations, accounting for dilution at plating, we estimate that a mixed infection would require both bacterial strains present at a level of 100 cells/ml of bacteria or more, and a pure infection would require at least 800 cells/ml of bacteria of one type and less than 100 cells/ml of the other. To calculate the likelihood of the data given a set of parameters, we simulate infections using our mixed stochastic-deterministic simulations. We repeat this 200 times to estimate the multinomial probabilities. We then write down the multinomial likelihood of the experimental data given the frequencies defined by the numerical simulations. Finally, we optimize the model over the parameters using `patternsearch` from Matlab with GPS Positive basis Np1 as the poll method. This routine allows optimization of stochastic functions. The optimization is performed at least three times from different initial conditions, and we report the best fit model as the one maximizing the likelihood over all such optimization runs.

The experimental data that we fit contains five different inoculum sizes, and three possible outcomes at 54 hrs post inoculation (for a total of 10 independent data points since the frequencies at each inoculum sum to one). In addition, the experimental data contains measurements a few minutes after inoculation for each inoculum size (10 more independent data points), at which point *every* infection was mixed. Note

that these data are not time series—every rat could be analyzed only once—so that the data at different time points are independently multinomially distributed.

These 20 data points must be explained by 8 independent parameters: α_j, g_G , d, N_0, r, γ, d_I, and ρ. This may sound like an easy fitting problem. However, it turns out that the requirement of having all mixed infections soon after inoculation, and a lot of pure infections later on is not easy to satisfy. Thus we do not perform formal analysis of the quality of fit / overfitting in this and the other models we try: the difficulty to fit the data makes most models obviously poor, and differences among the quality of fits of various models are clear without formal analyses.

The optimization is further constrained since biologically realistic limits exist on the model parameters. First, all of the parameters are positive. Further, an upper limit on N_0 is about $\sim 2 \times 10^9$ cells/ml [80], while its lower limit is determined by the fact that Moxon and Murphy observed as many as $\sim 1 \times 10^4$ cells/ml in the bloodstream of neonatal rats with severe infections [16]. The growth rate of *Hib* in synthetic blood culture was studied in [80], which provides the initial guess and upper limit of g_G between 0.4 to 1.2 per hour. We could not find any data in the literature regarding about the parameters of the innate immune response to *Hib*. However, some data is available for *Listeria* infection [81, 82], which allowed us to choose initial conditions of the immune response for the optimization: $r \sim 1 \times 10^{-6}$ h^{-1} cells^{-1}, $\gamma \sim 0.1$ h^{-1}, $d_I \sim 0.02$ h^{-1}.

Two of the best quantitative fits of the colloquial model are shown in Fig. 2.3. Some of the parameters of these fits are physiologically unrealistic, but even this does not help: none of the fits are good. The main difficulty seems to be that keeping the fraction of pure / indeterminate infections nearly constant over four orders of magnitude of the inoculum size, S, especially following a mixed infection soon after inoculation, is impossible within this independent action model. Indeed, the fit in the left panel keeps pure infections at nearly zero frequency in order to have few

mixed infections. Similarly, in the right panel, which does a better job in fitting the frequency of pure infections, the mixed infections rate spikes to 100% at high S. Note parenthetically that the non-monotonicity of the mixed infection line in this figure is because of the linearly increasing flux j. When $S = 10^4$ and 10^5, j is smaller than 1 bacteria per step. Therefore the number of bacteria is always zero and no immune cell is activated. When $S = 10^6$ and 10^7, both of strain A and B will have more than 100 bacteria due to the flux j in the end if no cell switches to growing phenotype and this is more often when $S = 10^6$. Even if any bacteria of A_C or B_G switches to the growing phenotype, the immune cells will clear the whole bacterial population is the swithcing happens too early and this is more often when $S = 10^7$. Therefore, when S increases from 10^6 to 10^7, the frequency of the mixed infections decreases but both of the frequency of the pure infections and indeterminates increase. When $S = 10^8$, however, all the infections are mixed because the flux j is so large that the immune response is not able to reduce the bacteria population below 100 at 54 hours post inoculation no matter there is switching or not.

2.3.2 Modifications to the colloquial model

One can slightly modify the model to make it fit better. Since rats have mucosal immunity [83, 84, 85, 86, 87], one can hope that bacteria in the nasopharynx will be eventually cleared as well. The simplest way of modeling this is to say that the flux from the nasopharynx into the bloodstream has a finite duration t_j, which itself is an unknown variable that needs to be fitted. Further, we notice that the natural (not caused by the immune system) death rate of bacterial cells and the death rate of immune cells in the fits in Fig. 2.3 are very small. Hence, to not overfit the data with the introduction of the new time parameter, we set both of these parameters to zero (we verified that the fits do not improve dramatically when this condition is relaxed). The optimized fit for this model is shown in Fig. 2.4. The fit is clearly better than in

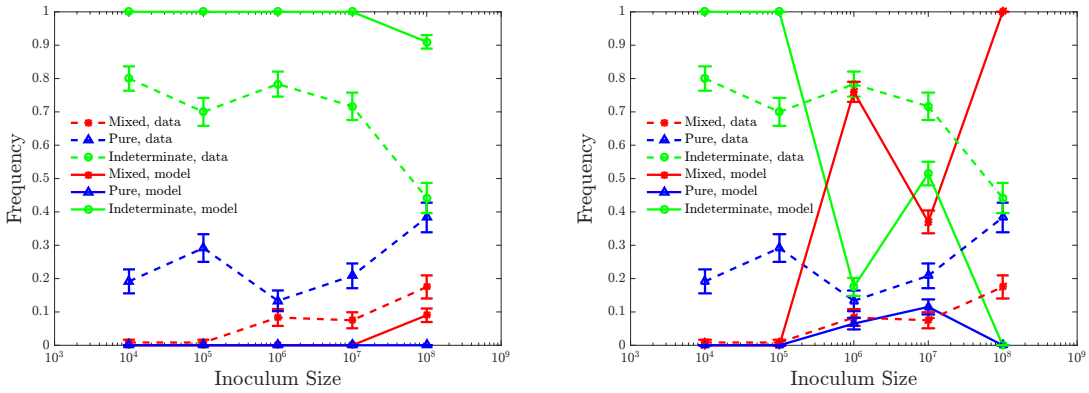

Figure 2.3: **Maximum likelihood fits of the colloquial model.** We show two different local maxima in the parameter space with nearly equivalent likelihoods. Neither provide quantitatively good fits. In this and subsequent figures, error bars on model predictions are given by standard deviations of results from 200 simulations. For the parameter values in the left panel ($\rho \approx 1.7 \cdot 10^{-5}\text{h}^{-1}$, $g_G = 1.0$ h^{-1}, $r \approx 6.1 \cdot 10^{-6}$ h^{-1} cells^{-1}, $\gamma \approx 240$ h^{-1}, $N_0 \approx 1.8 \cdot 10^9$ cells, $\alpha_j \approx 4.5 \cdot 10^{-5}$ h^{-1}, $d \approx 7.2 \cdot 10^{-4}$ h^{-1}, $d_I \approx 1.7 \cdot 10^{-6}$ h^{-1}), infections do not establish until very large inoculums. For the right panel ($\rho \approx 1.7 \cdot 10^{-5}$ h^{-1}, $g_G = 1.0$ h^{-1}, $r \approx 4.1 \cdot 10^{-8}$ h^{-1} cells^{-1}, $\gamma \approx 30.5$ h^{-1}, $N_0 \approx 1.2 \cdot 10^8$ cells, $\alpha_j \approx 1.2 \cdot 10^{-5}$ h^{-1}, $d = 0.01$ h^{-1}, $d_I = 0.018$ h^{-1}), the need to establish pure infections over the four orders of magnitude in the inoculum size leads to a large number of mixed infections as well.

Fig. 2.3, but it is still poor: to have pure infections at medium/high inoculums, the independent action hypothesis still requires no (or indeterminate) infections at small inoculums. All the infections are "Indeterminate" when the inoculum size is below 10^6. The flux is smaller than 10 cells per hour for $S = 10^4$ and 10^5, not enough to have one bacterial cell switching before the immune system kills all, or for a positive infection if no cell switches. When the $S = 10^6$, there is 14% probability to have a switching cell from one strain and establishing a pure infection, but not enough cells from the flux for a positive infection if no cell switches. When $S = 10^7$, the flux is large enough to be identified as a positive infection, as well as much larger chance to have bacterial cells from both strains switching to the growing phenotype. As soon as one cell from either strain switches, the immune response will rise exponentially and kill all cells from the other strain. However, the positive infections decrease when the inoculum size reaches 10^8. Given ten times more cells from the flux than $S = 10^7$, the

cells switch much earlier and activate the immune response much earlier. Note that the killing rate of immune cells is higher than the growth rate of the bacterial cells, 43.5% of the simulations end up with "Indeterminate" because there are not enough bacterial cells survived. The changes in the timing of switching events result in the inoculum size non-monotonically affecting the proportion of infections.

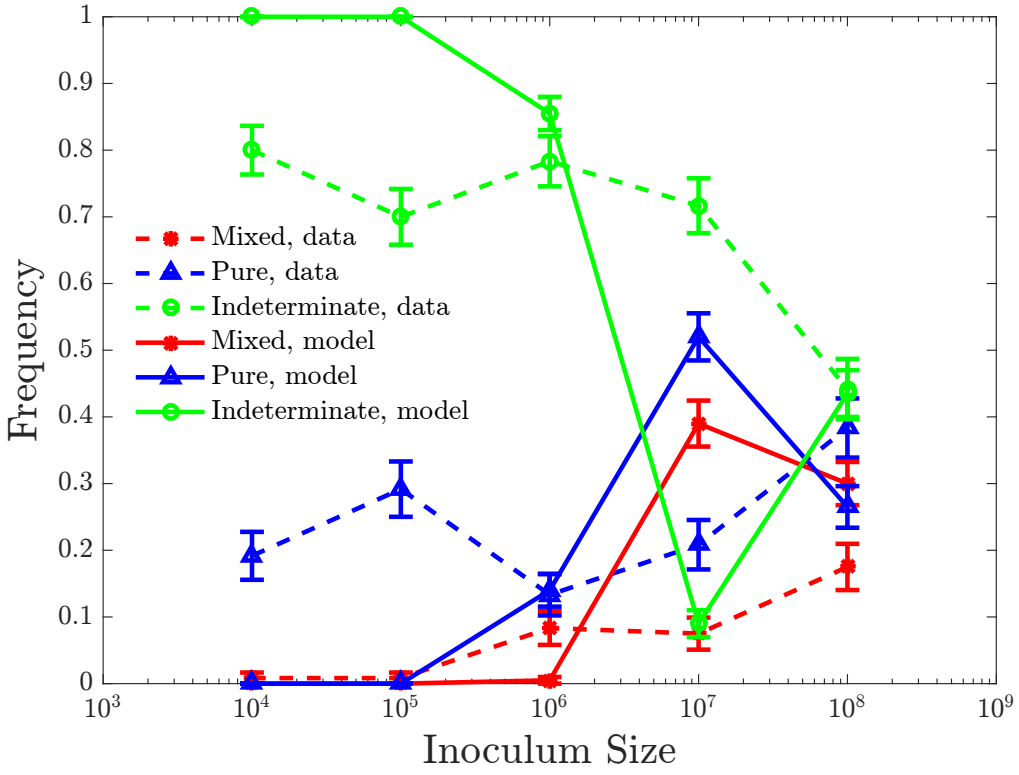

Figure 2.4: **Maximum likelihood fits of the colloquial model with the limited time duration of the bacterial flux from the nasal cavity to the bloodstream.** Natural bacterial cell death rate and immune cell death rate are set to zero. The duration of the flux is a fixed value for all inoculum sizes, $t_j \approx 4.1$ h. Other optimized parameters are: $\rho \approx 3.5 \cdot 10^{-5}$ h^{-1}, $g_G \approx 0.96$ h^{-1}, $\gamma \approx 2.0$ h^{-1}, $r \approx 2.1 \cdot 10^{-7}$ h^{-1} cells^{-1}, $N_0 \approx 1.0 \cdot 10^6$ cells, $\alpha_j \approx 1.4 \times 10^{-5}$ h^{-1}.

The key problem of the colloquial model is the experimentally observed weak dependence of the fractions of various infection types on the inoculum size. In other words, in simplest models, independent action means that the number of cells that attempt C→G switching in the blood scales with S. Thus the time to the first such

switch would scale as $1/S$. If the switch happens in the bulk of the 54 h experiment duration, an infection is established. Thus it is very hard to devise an independent action model that would have a non-negligible number of switches over 54 hrs at small inoculums ,$S = 10^4$, and yet would not have switches happening 100% of the time at large inoculums, $S = 10^8$. The model must be modified so that the mean time to the first switch decreases slower than $1/S$. Interestingly, there is a straightforward biologically realistic modification of the model that achieves this. In many cases, the process of bacterial phenotypic switching is not determined by a one-step chemical reaction, but proceeds through a series of roughly equally slow steps. For example, the switching of *E. coli* to express PAP genes and become virulent [88, 89] can be modeled as a four-step reaction [77]. Such n-step activation ensures that the probability distribution of time to the complete switch in an individual bacterium goes as $\propto t^{n-1}$ for small t [90, 91]. Then for $\propto S$ bacteria, the expected time till the first of them switches is governed by the Weibull distribution, resulting in $St^{n-1} \propto 1$, and $t \propto 1/S^{1/(n-1)}$ [91]. In other words, the time to the first bacterium in a large population switching scales sublinearly with the inverse population size, offering a potential opportunity to explain the weak dependence on the inoculum size.

We implement and optimized this model in numerical simulations by introducing a series of phenotypic transitions $\mathrm{C}\to\mathrm{G}_1 \to \cdots \to\mathrm{G}_n$, where only the last state, G_n, grows fast, and the rest of the states share the growth/death rates with C. Random switching between the subsequent states was again governed by the Poisson dynamics, as in Eq. (2.4). We explored $n = 2, 3, 4$. Fig. 2.5 shows results of the optimization, where $n = 3$, and all transition rates in the chain $\mathrm{C}\to\mathrm{G}_1 \to\mathrm{G}_2 \to\mathrm{G}_3$ were the same (which results in the most sublinear dependence of the switch time on S). Further, since in this model switching takes extended time, the first bacteria to cross over to blood from the nasopharynx will be the ones switching, and hence it makes little

difference for the switching statistics if the flux has a limited duration. At the same time, stopping of the flux into the blood results in a lower concentration of the non-switched strain, making it easier to develop pure infections at 54 hrs. Therefore, we inherit the value $t_j \approx 4.1$ hrs from the 1-step model. Clearly, the quality of fit improves dramatically compared to the 1-step model, and yet the fits are still far from perfect: mixed and pure infections go hand-in-hand, and to have no mixed infections at $S = 10^4$ requires having no infections at all at this inoculum. This illustrates a fundamental problem of the multi-step switching mechanism: while the time to a switch, indeed, scales sublinearly with $1/S$, the standard deviation of this time falls off very quickly, making the switching nearly deterministic [91]. Thus both strains switch at about the same time, and typically either both develop into an infection (mixed outcome) or none does (indeterminate outcome).

In summary, the independent action model, even augmented by multi-step switching and finite bacterial flux duration, seems to be incapable of explaining the observed experimental data.

2.3.3 Beyond the independent action model

The independent action hypothesis is implemented in our model by an assumption that the bacterial flux from the nasopharynx to blood is proportional to the inoculum size, S. We consider multiple extensions of the colloquial model that break this assumption.

First, we tried the model where the flux is independent of S, $j = \alpha_j$, which must be optimized. However, the flux duration scales nonlinearly with S, $t_j = \alpha_t S^{b_t}$. The logic behind this model is that there might be purely physical constraints on how many bacteria can cross the tissues between the two body compartment per unit time, and this bandwidth can be saturated even at moderate inoculums. At the same time, it could take the mucosal immunity a longer time to clear a larger inoculum. We

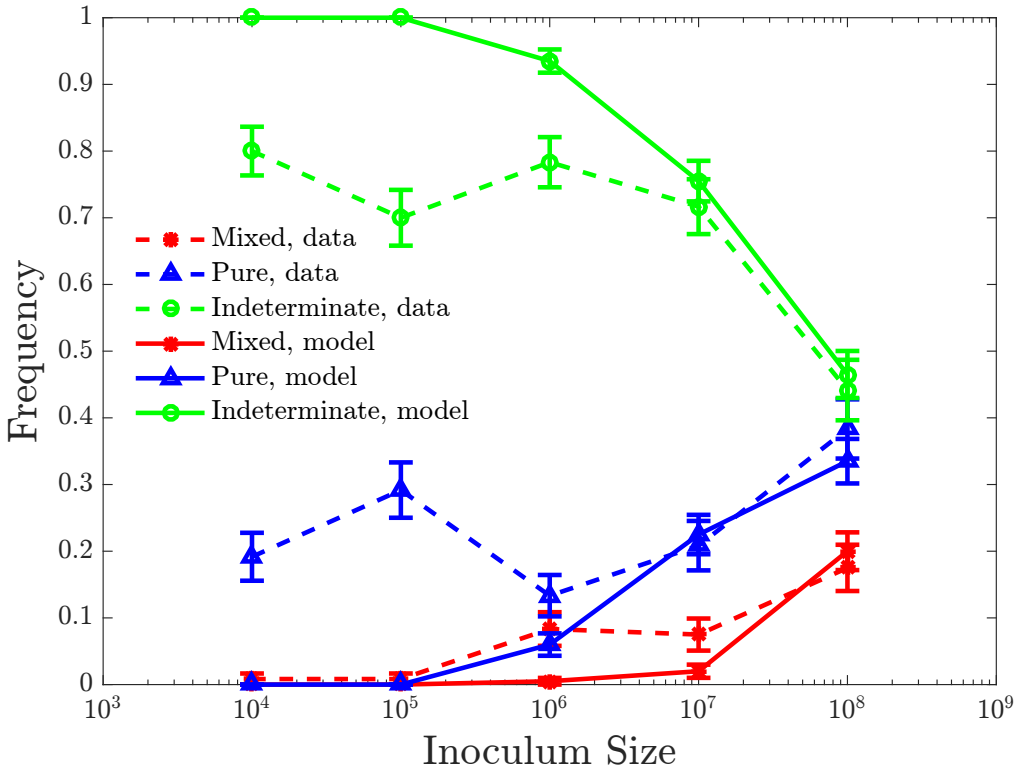

Figure 2.5: **Maximum likelihood fits for the colloquial model with the limited bacterial flux duration and three-step switching.** Natural bacterial cell death rate and immune cell death rate are set to zero. The duration of the flux is a fixed value for all inoculum sizes, $t_j \approx 4.0$ h. Optimized parameter values are $\rho \approx 0.0014$ h^{-1}, $g_G \approx 1.1$ h^{-1}, $\gamma \approx 9.7$ h^{-1}, $r \approx 1.1 \cdot 10^{-7}$ h^{-1} cells^{-1}, $N_0 \approx 1.0 \cdot 10^9$ cells, $\alpha_j \approx 3.4 \cdot 10^{-4}$ h^{-1}.

retain the 1-step switching model, because the higher variability of the switching time within this model allows for easier establishment of pure infections. The maximum likelihood results are shown in Fig. 2.6. While imperfect, the fits are surprisingly good, able to sustain pure, mixed, and indeterminate infections over the entire range of S. However, $b_t \approx 0.1$ is very small so that the duration of the bacterial flux is maximally ~ 3 hours, which makes it hard to imagine physiological mechanisms that would create it.

Another model that provides for non-independence is the model where the duration of the bacterial flux t_j is fixed and independent of S, but $j = \alpha_j S^{b_j}$. Optimized

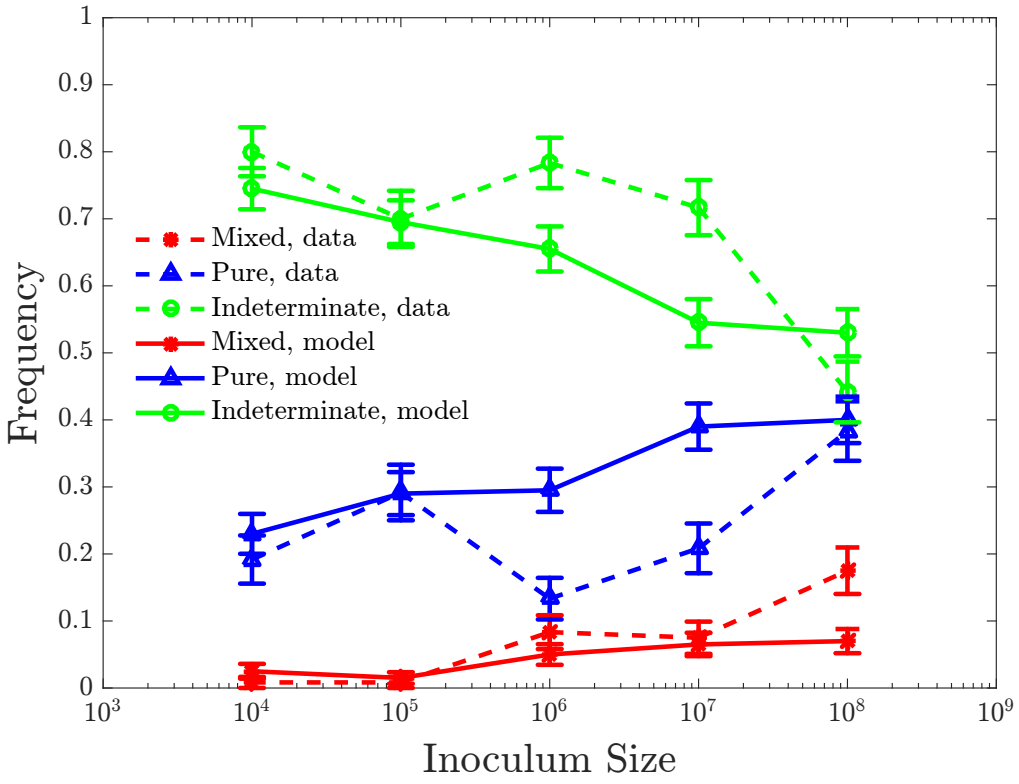

Figure 2.6: **Maximum likelihood fits for the non-independent action model with the S-dependent flux duration.** The fitted model has $j = \alpha_j = \text{const}$, and $t_j = \alpha_t S^{b_t}$. This model provides much better fits than all of the variants of the independent action model we have tested. The optimized parameters are $\rho \approx 6.1 \cdot 10^{-6}$ h^{-1}, $g_G \approx 0.55$ h^{-1}, $N_0 \approx 1.0 \cdot 10^7$ cells, $\gamma \approx 2.0$ h^{-1}, $r \approx 2.3 \cdot 10^{-6}$ h^{-1} cells^{-1}, $\alpha_t \approx 0.5$ h^{-1}, $b_t \approx 0.1$, $\alpha_j \approx 3.3 \cdot 10^3$ h^{-1}.

dynamics for this model is shown in Fig. 2.7, providing clearly the best fit to the experimental data. Interestingly, the fitted values of the parameters in this model are biologically realistic, resulting, for example, in bacterial fluxes of $10^2 \sim 10^3$ cells/h, and $t_j \approx 34$ hrs, longer than 1 day.

2.4 Discussion

In this work, we built mathematical models of early *Hib* infections started by a culture with two equally virulent bacterial strains. The models needed to account for the following broad observations: (1) both strains were present in the blood soon after the nasal inoculum; (2) most infections at different inoculum sizes either cleared from

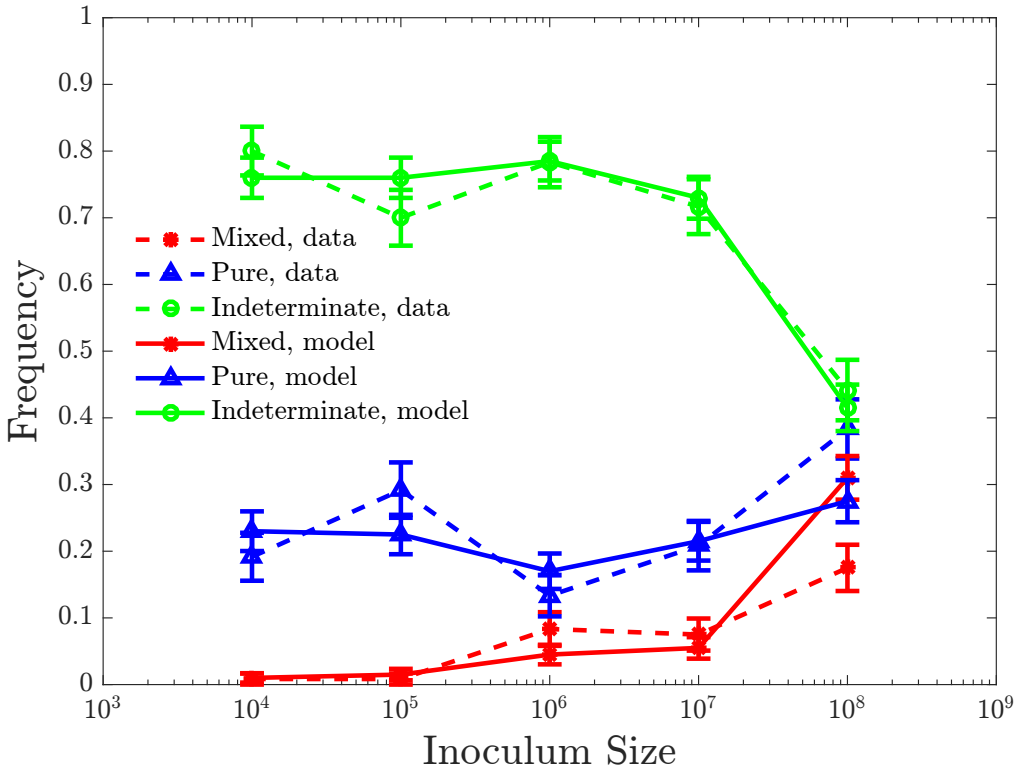

Figure 2.7: **Maximum likelihood fits for the non-independent action model with the sublinear dependence of the magnitude of the bacterial flux on** S**.**We assume $j = \alpha_j S^{b_j}$ with a fixed t_j. The optimized parameters are: $\rho \approx 5.7 \cdot 10^{-6}$ h^{-1}, $g_G \approx 1.0$ h^{-1}, $\gamma \approx 3.2$ h^{-1}, $r \approx 3.1 \cdot 10^{-6}$ h^{-1} cells^{-1}, $N_0 \approx 1.0 \cdot 10^6$ cells, $\alpha_j \approx 7$ h^{-1}, $b_j \approx 0.37$, and finally $t_j \approx 34.0$h, which is essentially equivalent to saying that the bacterial flux is temporally unconstrained.

the blood by 54 hrs post inoculation, or were pure—dominated by just one of the two strains; and (3) the dependence of the frequency of infection types (pure or mixed) on the inoculum size was very mild, changing at most a few-fold for a 10^4-fold change in the inoculum. The traditional colloquial explanation of these effects in the community has revolved around independent action of bacteria in establishing infections, with additional ingredients of stochasticity of phenotypic transitions, and the interactions with the immune system. Put simply, it is believed that both bacterial strains cross into the bloodstream, at which point one individual randomly switches into a faster growing phenotype and activates the immune system. In its turn, the immune system

clears out the non-switched strain, resulting in largely pure infections.

We analyzed this colloquial hypothesis quantitatively, starting with its simplest realization. Further, we considered additional variants that involved more complex (and hence statistically different) switching between the crossing and the growing phenotypes, or effects of mucosal immunity, which can clear the nasopharyngeal infection and stop bacterial flux into the bloodstream a few hours into the experiment. Surprisingly, none of these modifications was able to explain the experimental data, and specifically the weak dependence of the prevalence of infection types on the inoculum size. In contrast, when we forwent the independent action assumption and allowed the flux of bacteria into the bloodstream to depend sublinearly on the inoculum size, the fits to the data became very good. Thus our analysis suggests that the hypothesis of independent action may be violated in the case of early establishment of bacterial infections. Note that classic investigations of independent action [10] tested the hypothesis against *synergistic* effects. Here we argue that the non-independent action effects are redundant—the probability of a single bacterium to establish an infection decreases with the inoculum size. This is surprising, and certainly goes against ideas in the quorum sensing literature [92], where an infection is established synergistically when the number of bacteria crosses a certain quorum threshold.

Our best model suggests that the flux of bacteria from the nasopharyngeal inoculation to the bloodstream scales as the inoculum size to the ~ 0.37 power. The amount of data we have does not allow us to propose verifiable explanations for the mechanism of this scaling: the physical structure of the animal tissues, the fluid dynamics of the bacterial culture in the nasopharyngeal cavity, interactions of bacteria with the immune system, or interactions of bacteria among themselves could all play a role. The closeness of the exponent to $1/3$ is also interesting, suggesting that maybe a certain modification of the 3-step stochastic switching model, similar to that studied in Fig. 2.5, could play a role as well.

It is hard to establish negative results in scientific studies. This is partly because of social pressures [93], but also because of an objective difficulty: one can never be sure that the negative result is meaningful, rather than due to not trying hard enough to find a possible explanation to the data. Similarly, in our study, we cannot be sure that we have explored the parameter space well enough, and that we have tried all simple, reasonable modifications to the original colloquial model to argue that the independent action theory cannot explain the data. We can only say with certainty that *we could not reconcile* the independent action theory with the data, which is a much weaker statement. It will take many additional investigations, experimental and theoretical, to understand if and under which conditions the independent action hypothesis is, indeed, violated in early infections. We hope that our study will spur such future investigations.

CHAPTER III

ANTIBIOTIC SUSCEPTIBILITY OF BACTERIAL COLONIES: AN ASSAY AND EXPERIMENTS WITH *STAPHYLOCOCCUS AUREUS*

(This chapter is based on "Shao, X., Kim, J., Jeong, H. J., & Levin, B. (2016). Antibiotic susceptibility of bacterial colonies: An assay and experiments with *Staphylococcus aureus. submitted.*")

3.1 Introduction

The rational (as opposed to purely empirical) approach to determining antibiotics and dosing regimens is based on estimates of the changes in the serum concentration of the drugs following their administration, pharmacokinetics (PK) and the relationship between the concentration of the drug and the rates of growth and death of the target bacteria, pharmacodynamics (PD) [94, 95, 96, 97, 98]. Almost all we know about the PDs of antibiotics and bacteria is from *in vitro* studies of planktonic cells maintained in well-agitated liquid cultures and the theoretical analog of these culture conditions. Mathematical and computer simulation models of PDs also assume an effectively dimensionless habitat and mass action processes [99, 100, 101, 102, 103, 104, 105, 106, 107]. Under these conditions all the bacteria in a population have equal access to each other as well as resources, wastes, and allopathic agents like antibiotics.

In the real world of infections, however, bacteria are more likely to live in physically structured habitats, embedded in polysaccharide matrices known as biofilms adhered to surfaces or as colonies on top of tissue surfaces or within semi-solids

[24, 26, 108]. Contrary to laboratory conditions, the bacteria within these physically structured habitats vary in access to resources as well as the concentrations of antibiotics that confront them. How does this inconvenient reality of physically structured habitats affect the pharmacodynamics of antibiotics? And if there is an effect on pharmacodynamics, are our current standards for designing and evaluating antibiotics unrepresentative of *in vivo* conditions?

Methods have been developed for the *in vitro* study of elements of the pharmacodynamics of antibiotics and bacteria in biofilms [25, 32, 34, 108, 109, 110, 111, 112, 113, 114]. Nevertheless, *S. aureus* has always been among the most concerning of pathogens for skin infections, in addition to nasal colonization and lung infections [24, 25, 26]. The population dynamics of these circumstances are quite different from those studied in biofilms which are formed under continuously flowing fluid. To our knowledge, there are few published methods to study pharmacodynamics of antibiotics for *S. aureus* as discrete colonies.

In this report, we present a method to quantitatively evaluate the antibiotic susceptibility of bacteria growing as colonies on surfaces and compare their susceptibility to planktonic bacteria of the same densities and physiological state. Using this method we explore the susceptibility of *Staphylococcus aureus* Newman growing as colonies to antibiotics of different classes, including six bactericidal antibiotics which are ciprofloxacin, gentamicin, vancomycin, oxacillin, ampicillin and daptomycin, and three bacteriostatic antibiotics which are tetracycline, erythromycin and linezolid. We investigated the effect of physiological state of cells and the physical structure of colonies on the efficacy of antibiotics. The results of our study indicate substantial variation in the efficacy of the tested antibiotics to treat *S. aureus* maintained as colonies. Antibiotics that are effective in killing *S. aureus* in liquid culture are virtually ineffective when these bacteria are growing as colonies.

3.2 Materials and Methods

3.2.1 Bacteria

Staphylococcus aureus Newman was used in this investigation, which was a generous gift from William Shafer. This strain has a clinical origin, remains virulent and has been extensively used in studies of staphylococcal pathogenicity (20).

3.2.2 Media

The grow medium for *S. aureus* Newman was made with Cation Adjusted Mueller-Hinton II Becton Dickinson (Franklin Lakes, NJ, USA). Cell densities were estimated by plating on LB agar plates. Lysogeny Broth (LB) Becton Dickinson, (Franklin Lakes, NJ, USA) was used to prepare these LB agar plates.

3.2.3 MIC determination

Minimum Inhibitory Concentrations (MICs) were estimated using a serial-dilution protocol modified from that discribed by *CLSI* in [115]. Initial cell numbers of 5×10^7 cells/ml and the standard 5×10^5 cells/ml were inoculated into MHII liquid broth with antibiotics. In order to ascertain more precise estimates of the MICs, we used different starting concentrations of the antibiotics in our serial-dilution protocol. The determined values for MICs are listed in Table. 1.

3.2.4 Procedure for the colony assay of antibiotic efficacy and liquid culture controls.

In Fig. 3.1, a step-by-step diagram illustrates how to prepare the bacterial colonies grown on surfaces, expose the these cells to antibiotics and evaluate the viable cell densities.

3.2.4.1 Establishing the liquid cultures and colonies

Inoculation cells of *S. aureus* Newman were obtained from overnight cultures with MHII broth. To prepare bacterial colonies, 3 ml of 1.6% agar with 0.1X MHII were

Table 1: **Antibiotics' sources and MICs in MHII liquid broth with different inoculum densities.** The MICs of nine antibiotics in MHII broth of different concentrations and cultures initiated with different numbers of viable cells, unit of the concentrations is in μg/ml.

Antibiotics	**Source**	5×10^5 **cells/ml**	5×10^7 **cells/ml**
Vancomycin	hydrochloride, Sigma	1.3	3.5
Gentamicin	AppliChem	0.9	1.1
Ciprofloxacin	AppliChem	0.3	0.3
Daptomycin	TCI	1.3	4.0
Ampicillin	Sigma	0.9	1.3
Oxacillin	Sigma	0.2	0.5
Tetracycline[*]	Sigma	0.5	
Erythromycin[*]	MP Biomedicals	0.5	
Linezolid[*]	Chem-IMPEX	1.1	

[*] We have not included the effects of inoculation densities on the MICs of the bacteriostatic antibiotics because the results of our experiments in Tbl. 2 and Tbl. 3 suggested that the density of the exposed bacterial population does not contribute to the susceptibility of colonies to the action of these drugs.

aliquoted into the wells of Costar Macrotiter 6-well plates. After the agar hardened, Tuffryn ^{TM} filters were put onto the agar in each well. Certain amount of cells were inoculated onto the filters and spread using a glass rod spreader. The 6-well plates were then incubated at 37°C for 24 or 48 hours (Fig. 3.2). Same amount of cells from the overnight culture were inoculated into 0.1X MHII liquid broth in parallel but with continuous shaking.

3.2.4.2 Exposing the bacteria to antibiotics

To ascertain the efficacy of antibiotics on intact colonies, 3 ml of 1.6% agar with standard concentration of MHII were aliquoted into the wells of Costar Macrotiter 6-well plates. These agar media either contain 10X MIC of antibiotics or no antibiotics as controls. Filters incubated for 24 or 48 hours were transferred onto these agar and incubated at 37°C for additional 5 or 24 hours before sampling. In parallel, the cells from the 24-hour or 48-hour old liquid cultures were inoculated into liquid MHII broth with 10X MIC antibiotics or antibiotic-free controls. The dispersed cultures

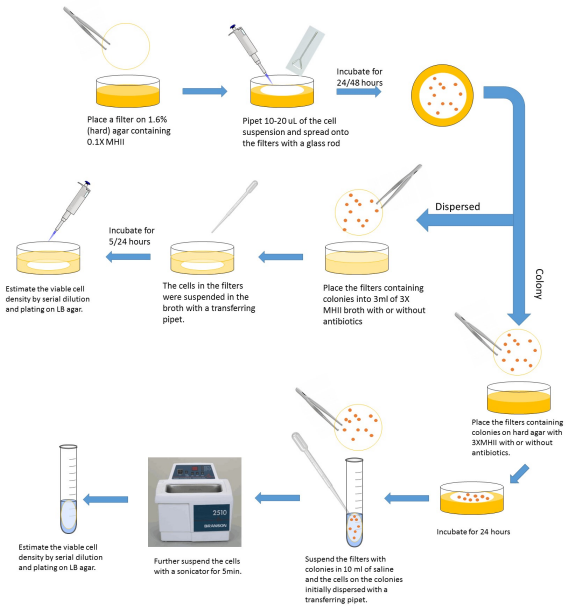

Figure 3.1: **The experiment setup and protocol to grow and treat *S. aureus* Newman grown as colonies on filters.** The growth of bacterial colonies is the same for the colony cultures and the dispersed cultures. After 24 or 48 hours of growth, the filters with bacterial colonies are transferred and washed into fresh liquid MHII broth containing antibiotics for the dispersed cultures. Or the filters are maintained intact and tranfer onto fresh agar containing MHII media and antibiotics.

were prepared as the following procedure: the filters with 24-hour or 48-hour old colonies were transferred into 3 ml of 3X MHII broth with or without antibiotics in the wells of Macrotiter plates. The cells on the filters were washed and mixed into the broth using a transferring pipette. The filters were in the broth and the plates were then incubate at 37°C with continuous shaking for 5 or 24 hours. An example of dispersed cultures is shown in Fig. 3.2.

3.2.4.3 Sampling and evaluating the viable cell densities

The sampling of liquid cultures and dispersed cultures were followed by serial dilution and plated on LB agar plates and count the colony forming units (CFUs). The filters with colonies were sampled as shown in Fig. 3.1. Each filter was transferred into 10ml of 0.85% saline. The colonies on filters were washed and dispersed into saline

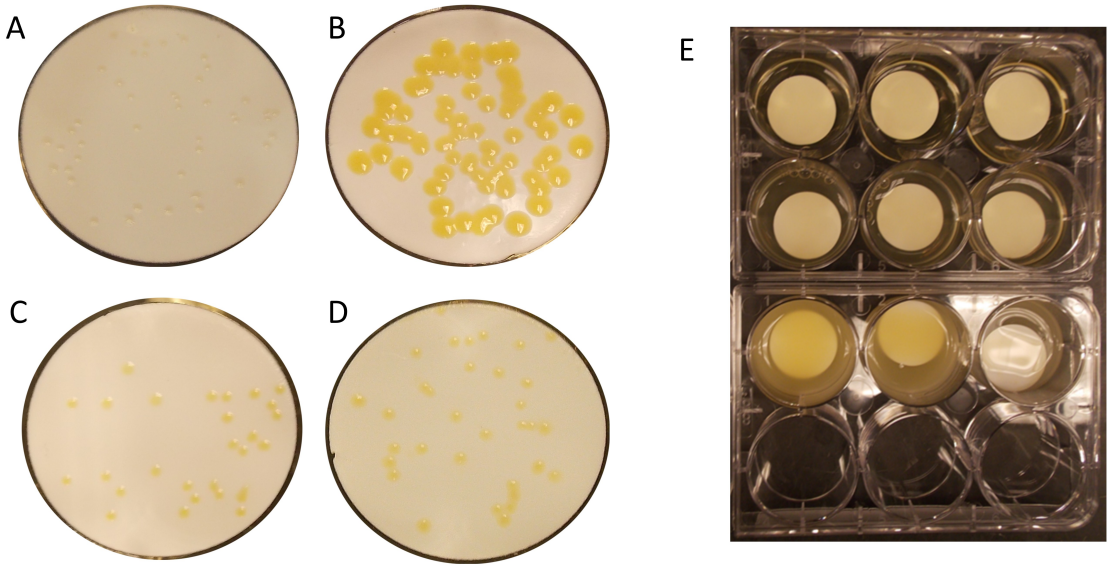

Figure 3.2: ***S. aureus* Newman grew as colonies on filters. Approximately 50 colonies were inocultated on each filter.** (A) a COL-0 sample. The colonies were incubated for 48hours on 3 ml of 0.1x MHII agar (48h-old colonies). The diameter of the colonies were about 0.6∼0.8mm (B) a COL-CON sample, 48h-old colonies were transferred onto 3 ml of 3x MHII agar and incubated for an additional 24hours. The colonies were large and yellow, diameter 1.6∼2.5mm. (C): COL-OXY48+24, 48h-old colonies were transferred onto 3 ml of 3X MHII agar with 10X MIC oxacillin and incubated for an additional 24hours, not significant larger but more colored than (A), diameter 0.7∼1.0mm. (D) COL-CIP48+24, 48h-old colonies were transferred onto 3 ml of 3x MHII agar with 10X MIC ciprofloxacin and incubated for another 24hours, larger and more colored, diameter 0.8∼1.1mm. (E) Dispersed cultures transferred from 48h-old colonies and exposed to fresh media for 24hours. From top row to bottom row are DIS-CIP, DIS-OXA, DIS-CON, turbidity increasing.

using a transferring pipette, until no visible colonies could be seen. To fully break up clumps and take off cells from the filters, the saline suspensions were sonicated for 5 minutes and vortexed for 10 seconds, followed with serial diluion and plating on LB agar plate. The sonicator was from Bronson, 2510R-DTH, output 100W, 42 kHz±6%.

3.3 Results

3.3.1 Resource saturation of *S. aureus* Newman in liquid cultures and as colonies.

The efficacy of antibiotics depends largely on the physiological states of the bacterial cells [116], which is reflected in the growth rates of cells and the cell density of the population. To explore these effects of the bacterial population before exposure to antibiotics, we evaluated the cell densities of bacteria as colonies and in liquid culture. We compared the bacterial growth with different inoculum sizes at 24 hours (Fig. 3.3 blue bars) and 48 hours(Fig. 3.3 orange bars) in 0.1X MHII medium or 3X MHII medium.

Among the liquid cultures with 0.1X MHII, there is no significant effect of the inoculum size on the cell density of *S. aureus* Newman at 24 or 48 hours ($p\sim 0.9$) (Fig. 3.3 A). All these cultures saturated before 24 hours. We would expect that the cells in these cultures would have already reached stationary phase when exposed to antibiotics in our later experiments. The liquid cultures with 3X MHII, however, were still growing at 24 hours and presumingly saturated at 48 hours since they all reached at the same level of cell densities($p\gg 0.05$) (Fig. 3.3C). When *S. aureus* Newman grown as colonies, all the cultures were still growing at 24 hours at 24 hours on both 0.1X MHII and 3X MHII agar (Fig. 3.3 B and D) and thereby larger colonies is still growing, whilst those inoculated with 10^3 and 10^4 cells appear to be at stationary phase. At 48 hours the population inoculated with 50 cells per filter were still smaller than that with 10^3 and 10^4 cells per filter and thereby larger colonies is

still growing, whilst those inoculated with 103 and 104 cells appear to be at stationary phase ($p \gg 0.05$).

We interpret these results to mean that when liquid cultures in 0.1X MHII are exposed to antibiotics, they are already at stationary phase at 24 hours, but in 3X MHII they are still growing. At 48 hours with inoculates of 10^3 and 10^4 cells, these colonies are no longer growing and presumably the cells are at stationary phase, which is not the case for cultures initiated with 50 colonies. It should be noted that, at 48 hours, the cell densities of the colony cultuers on 0.1X MHII inoculated with 10^3 and 10^4 cells per filter was about 2 fold of the cell densities of the corresponding liquid culture. Similar observations were reported in [54, 117], especially when the resource is limited in the habitat. This is not the case for the richer media, 3X MHII, where there is no significant difference in the 48 hour estimated densities when the bacteria are growing in liquid or as colonies ($p \gg 0.05$).

3.3.2 The effect of physiological states of cells grown as colonies on the susceptibility of these cells to antibiotics

Given the analysis of physiological states of *S. aureus* Newman with different initial cell densities and at different times, we conducted the experiments to explore the effect of these features on the PD of antibiotics on bacterial cells as colonies and compare with liquid controls. Of particular interest are the questions including: (i) How does the size (number of cells within and the physical dimensions) of colonies affect their susceptibility to killing by antibiotics? (ii) How does the distance between colonies, the density on the agar affect their susceptibility to killing by antibiotics? (iii) Most importantly, how effective are different antibiotics in inhibiting the growth and killing of *S. aureus* in liquid and within colonies? To address these questions, we compared the colonies culture inoculated with 50 and 10^4 cells per filter, respectively the large, distanced colonies and the small , crowed colonies (Fig. 3.4). The filters with colonies were incubated for 24 hours or 48 hours before transferring onto 1X

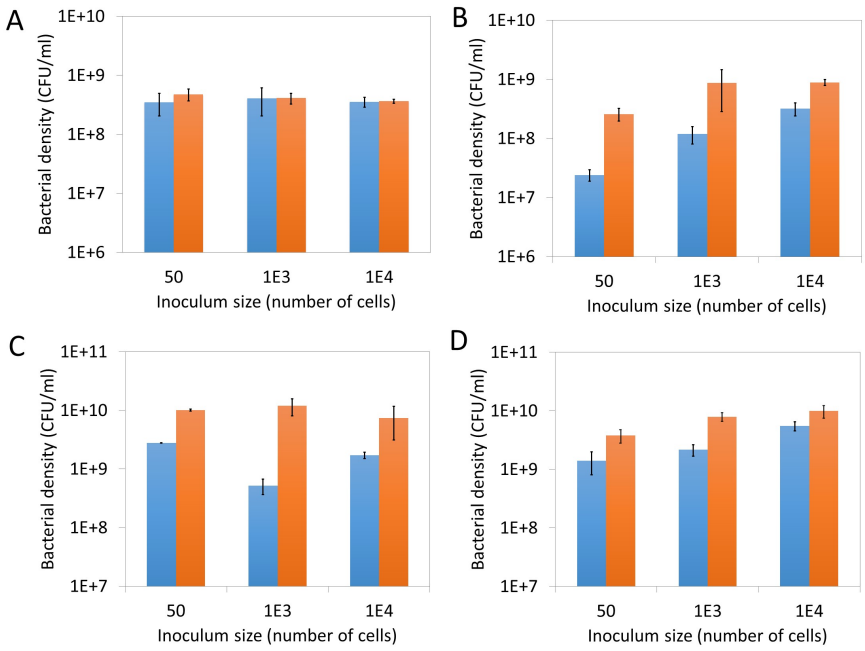

Figure 3.3: **Assessment of physiological states of *S. aureus* Newman cells as colonies and in liquid culture at 24 and 48 hours.** Cultures were inoculated with 50, 10^3 and 10^4 cells per filter or per 3 ml of liquid culture respectively. Viable cell density of *S. aureus* Newman at 24 (blue bars) and 48 (orange bars) hours grown as (A) planktonic cells in liquid culture with 0.1X MHII, (B) colonies on filters on agar with 0.1X MHII, (C) planktonic cells in 3X MHII broth, and (D) colony on filters on 3X MHII agar. Error bars are SEMs.

Figure 3.4: ***S. aureus* Newman grew as small and crowded colonies.** Initial cell density was 10^4 cells per filter. Filter with cells were incubated on 0.1X MHII agar for 48 hours.

MHII agar containing 10X MIC of one of the nine antibiotics introduced in Section. *Methods and Material*.

The experimental results are shown in Table 2 and Table 3. In the absence of antibiotics, both of cells grown in liquid cultures and as colonies were able to replicate after being transferred to new broth or on to new agar, despite the age or the inoculum size of the cultures. Among the six bactericidal antibiotics, ciprofloxacin was the most effective in killing both planktonic *S. aureus* cells in liquid cultures and those as colonies. In Table 2, bacterial cells within the younger, 24-hour old colonies were even more susceptible to this fluoroquinolone than the corresponding liquid culture, but became much more refractory when the colonies get older, *i.e.* at 48 hours. This was also the case for gentamicin, where young and old colonies showed dramatically difference in the susceptibility to this antibiotic, comparing to liquid cultures. The two beta-lactam antibiotics were less effective in killing *S. aureus* in colonies than they were dealing with plancktonic cells in liquid. Vancomycin was moderately bactericidal in liquid but totally ineffective when bacteria were in colonies. At these densities,

daptomycin was effectively bacteriostatic in both liquid and younger colonies and even allowed for the growth of the 48hour colonies. And the three bacteriostatic antibiotics managed to inhibit the cell growth in all cultures. It has been shown that the efficacy of daptomycin and vancomycin on *S. aureus* strongly depends on the cell density [118, 119]. Thus the failure of these two antibiotics may be closely related to the relatively high cell density of the culture when exposed to the antibiotics and the degradation of these drugs at this great cell densities.

In treating the cultures initiated with 10^4 cells per filter or per 3 ml of liquid broth, ciprofloxacin was again the most effective among these nine antibiotics, followed by gentamicin. These two drugs showed slightly higher efficacy in killing the 24-hour old colonies, comparing to the young colonies initiated with 50 cells. Ampicillin was still weakly effective in inhibiting colonies growth, while oxacillin failed to do so to the 48-hour old colonies. Vancomycin and daptomycin simply failed to treat the colonies and allow for their growth. Surprisingly, all the three bacteriostatic antibiotics remained effective in all colonies cultures but failed to inhibit the growth of bacteria in all liquid cultures.

3.3.3 The effect of the physical structure of bacterial colonies on the susceptibility of these cells to antibiotics

The previous section shows that the bacterial cells within colonies are generally more refractory than those in liquid cultures. Besides the contribution of physiological state, we also considered the effect from the physical structure of the colonies. Whether does the diffusion of the antibiotics hindered by the polysacchride matrix of colonies? Are the cells more refractory in colonies due to some protection from the colonies structure? To evaluate the contribution of the physical structure of the colonies to these antibiotics, we evaluated the efficacy of ciprofloxacin and oxacillin in treating *S. aureus* grown as colonies, and compared with colonies with that of planktonic cells released from colonies (dispersed, DIS) and liquid cultures (LIQ) of the

Table 2: The results of experiment with *S. aureus* Newman cultures initiated with an average of 50 colonies per 3 ml of MHII broth/agar containing 10X MIC of the drugs listed. Cultures grew for 24 or 48 hours in 3 ml of 0.1X MHII broth/agar before exposure to the antibiotics in 1X MHII. The viable cell densities (CFUs/ml) were estimated 24 hours after exposure to the antibiotics.

50C	**24-hour growth**		**48-hour growth**	
	Liquid	**Colony**	**Liquid**	**Colony**
Initial	$2.2 \pm 0.1 \times 10^7$	$2.7 \pm 0.2 \times 10^7$	$1.9 \pm 0.1 \times 10^7$	$2.7 \pm 0.2 \times 10^8$
Control	$4.4 \pm 1.0 \times 10^9$	$5.3 \pm 0.6 \times 10^9$	$4.6 \pm 0.9 \times 10^9$	$5.3 \pm 0.7 \times 10^9$
Ciprofloxacin	$9.7 \pm 1.0 \times 10^3$	$7.4 \pm 1.1 \times 10^2$	$5.0 \pm 5.0 \times 10^2$	$5.5 \pm 0.6 \times 10^6$
Gentamicin	$9.1 \pm 0.4 \times 10^4$	$1.2 \pm 0.1 \times 10^4$	$1.6 \pm 0.3 \times 10^4$	$1.7 \pm 0.3 \times 10^8$
Ampicillin	$7.0 \pm 3.0 \times 10^3$	$1.3 \pm 0.1 \times 10^5$	$1.0 \pm 1.0 \times 10^3$	$1.1 \pm 0.2 \times 10^8$
Oxacillin	$1.8 \pm 0.1 \times 10^5$	$4.9 \pm 1.0 \times 10^6$	$7.4 \pm 2.3 \times 10^4$	$2.1 \pm 0.2 \times 10^8$
Vancomycin	$3.1 \pm 1.4 \times 10^4$	$1.6 \pm 0.6 \times 10^8$	$6.1 \pm 1.1 \times 10^5$	$4.0 \pm 0.4 \times 10^9$
Daptomycin	$4.1 \pm 0.3 \times 10^6$	$1.5 \pm 0.4 \times 10^7$	$1.6 \pm 0.8 \times 10^7$	$3.9 \pm 0.7 \times 10^8$
Tetracycline	$1.2 \pm 0.3 \times 10^6$	$8.0 \pm 1.0 \times 10^6$	$4.1 \pm 0.9 \times 10^6$	$2.5 \pm 0.3 \times 10^8$
Erythromycin	$4.6 \pm 0.5 \times 10^6$	$6.0 \pm 0.3 \times 10^6$	$2.3 \pm 0.6 \times 10^7$	$2.4 \pm 0.3 \times 10^8$
Linezolid	$1.6 \pm 0.3 \times 10^6$	$7.7 \pm 0.4 \times 10^6$	$1.4 \pm 0.1 \times 10^7$	$2.2 \pm 0.2 \times 10^8$
Color map instructions				
	Stasis or growth			
	Viable cell density decrease less than an order of magnitude			
	Viable cell density decrease between 1 and 4 orders of magnitude			
	Viable cell density decrease >4 orders of magnitude			

Table 3: The results of experiment with *S. aureus* Newman cultures initiated with an average of 10^4 colonies per 3 ml of MHII broth/agar containing 10X MIC of the drugs listed. Cultures grew for 24 or 48 hours in 3 ml of 0.1X MHII broth/agar before exposure to the antibiotics in 1X MHII. The viable cell densities (CFUs/ml) were estimated 24 hours after exposure to the antibiotics.

10^4**C**	**24-hour growth**		**48-hour growth**	
	Liquid	**Colony**	**Liquid**	**Colony**
Initial	$1.4 \pm 0.6 \times 10^7$	$3.2 \pm 0.2 \times 10^8$	$1.4 \pm 0.3 \times 10^7$	$8.9 \pm 0.3 \times 10^8$
Control	$3.4 \pm 0.4 \times 10^9$	$8.2 \pm 2.2 \times 10^9$	$2.5 \pm 0.2 \times 10^9$	$1.2 \pm 0.1 \times 10^{10}$
Ciprofloxacin	$6.5 \pm 6.5 \times 10$	$1.0 \pm 0.2 \times 10^3$	$2.8 \pm 0.1 \times 10^7$	$9.3 \pm 1.3 \times 10^5$
Gentamicin	$1.2 \pm 1.2 \times 10^2$	$1.9 \pm 0.6 \times 10^5$	$3.0 \pm 2.5 \times 10^6$	$3.5 \pm 0.9 \times 10^7$
Ampicillin	$9.8 \pm 1.8 \times 10^4$	$5.2 \pm 0.8 \times 10^7$	$1.35 \pm 0.8 \times 10^8$	$2.7 \pm 0.6 \times 10^8$
Oxacillin	$4.8 \pm 4.6 \times 10^5$	$5.8 \pm 0.9 \times 10^7$	$2.7 \pm 1.9 \times 10^8$	$2.7 \pm 0.2 \times 10^9$
Vancomycin	$3.4 \pm 0.9 \times 10^7$	$5.6 \pm 0.2 \times 10^9$	$2.5 \pm 0.5 \times 10^8$	$7.7 \pm 0.9 \times 10^9$
Daptomycin	$3.6 \pm 0.4 \times 10^5$	$2.3 \pm 0.5 \times 10^9$	$6.3 \pm 2.1 \times 10^6$	$1.7 \pm 0.1 \times 10^9$
Tetracycline	$3.3 \pm 0.6 \times 10^8$	$8.8 \pm 0.5 \times 10^7$	$1.2 \pm 0.6 \times 10^9$	$6.1 \pm 0.5 \times 10^8$
Erythromycin	$3.0 \pm 0.5 \times 10^8$	$7.3 \pm 0.6 \times 10^7$	$1.1 \pm 0.2 \times 10^9$	$2.2 \pm 0.3 \times 10^8$
Linezolid	$4.0 \pm 0.5 \times 10^8$	$1.2 \pm 0.2 \times 10^8$	$9.0 \pm 1.9 \times 10^8$	$5.5 \pm 0.3 \times 10^8$
Color map instructions				
	Stasis or growth			
	Viable cell density decrease less than an order of magnitude			
	Viable cell density decrease between 1 and 4 orders of magnitude			
	Viable cell density decrease >4 orders of magnitude			

same age as the colonies . All cultures were treated with 3X MHII broth or agar containing 10X MIC of these drugs and the viable cell densities were estimated after 5 and 24 hours of exposure to the antibiotics. In Fig. 3.2, we illustrate the experimental setup and the effects of exposure on the size of 48-hour colonies in the absence of antibiotics and following exposure to oxacillin and ciprofloxacin.

Both the 24-hour and 48-hour old cultures resumed to replicate in the absence of antibiotics(CON in Fig. 3.5), and the size of colonies and the pigmentation dramatically increased (Fig. 3.2). In younger cultures, those grown for 24 hours, a substantial fraction of the population exposed to 10XMIC ciprofloxacin was killed by 5 hours, with the greatest killing in LIQ-CIP and lowest in COL-CIP. After 24 hours of exposure, the bacteria within colonies or dispersed from colonies appeared more sensitive to killing by this fluoroquinolone than those in liquid culture ($p \ll 0.05$) (Fig. 3.5A). After 48 hours of growth, the bacteria within colonies are more refractory to ciprofloxacin than they are as planktonic cells. For both the 24 and 48-hour cultures, relative to the antibiotic-free controls, ciprofloxacin was effective in preventing the growth and killing *S. aureus* with colonies.

Oxacillin was clearly less effective than ciprofloxacin in killing *S. aureus* in planktonic cells as well as within colonies. After 24 hours of exposure, there is about 10 to 100 fold reduction in the viable cell density with the greatest reduction in DIS-OXY. Moreover, there appeared to be little difference in the efficacy of this beta-lactam antibiotic in killing *S. aureus* in colonies relative to that of planktonic cells in liquid. This experiment was repeated three times and similar results obtained (data available upon request).

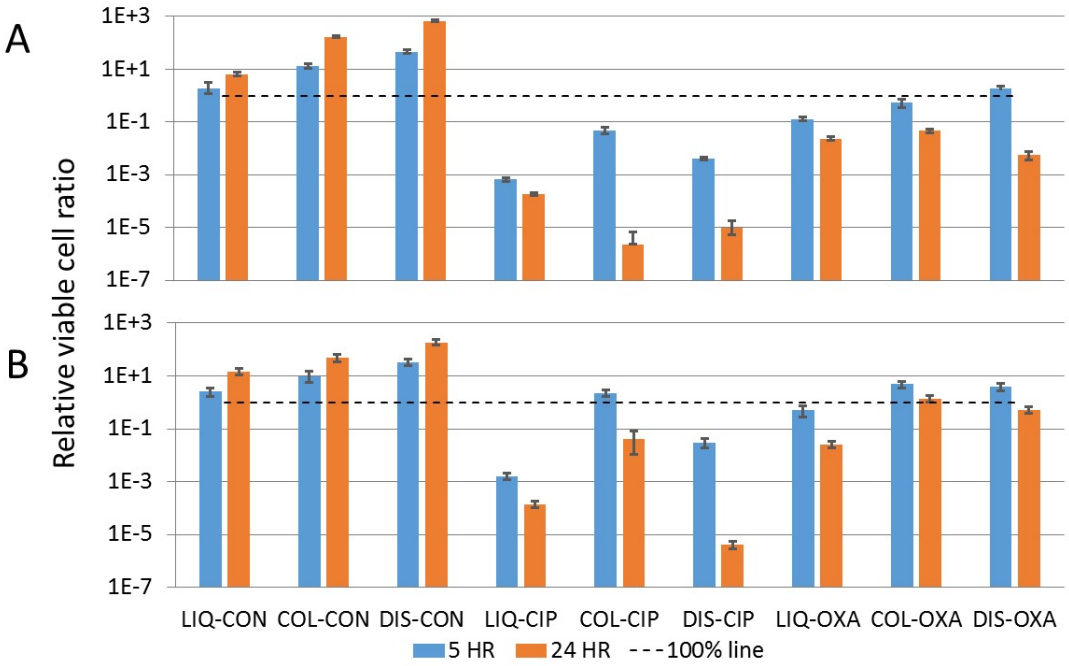

Figure 3.5: Relative survival of *S. aureus* exposed to 10XMIC ciprofloxacin (CIP) or oxacillin (OXA), in liquid cultures(LIQ), as planktonic cells dispersed from colonies (DIS), and as intact colonies (COL). An average of 50 colonies was inoculated on each filter. The CON cultures are antibiotic-free control. Means and standard errors for three replicates. A- Cultures grown for 24 hour before exposure to the antibiotic, B- Cultures grown for 48 hours before exposure to the antibiotic. Viable cell density was measured at 5 hours after exposure (blue bars) and at 24 hours after exposure (red bars). Dashed lines represent the cell densities before transferring as a guideline.

3.4 Discussion

Our method of developing bacterial population as colonies on filter membranes is designed to be facile, and can be broadly applied to more complex experimental set-ups. We evaluated this method by applying it to investigate the population growth of *Staphylococcous aureus* Newman and the pharmacodynamics of nine different antibiotics on this strain of bacteria. We explored the contribution of physiological states of the cells and the physical structure of the colonies to the efficacy of antibiotics. While there have been a number of studies of the efficacy of antibiotics for treating bacteria in biofilms [32, 34, 109, 110, 111, 114, 120, 121, 122, 123], to our knowledge this is the first investigation to explore antibiotic-mediated inhibition of replication and killing of bacteria growing as discrete colonies on surfaces.

The procedure developed here can be applied to virtually any bacteria that when grown *in vitro* forms colonies. This same procedure could be employed to evaluate the susceptibility of single and multi-species biofilms to antibiotics. For this, instead of seeding the filters with relatively few bacteria to form discrete colonies, the filters could be seeded with large numbers of bacteria of the same or multiple species. The sampling methods would be identical to those described in here. By comparing liquid cultures and bacteria released from colonies (or biofilms) of the same density and stage of growth (age) this method provides a way to evaluate the contribution of the physical structure of the population to its susceptibility to antibiotics.

The results of this study indicate that there is substantial variation among bactericidal antibiotics in their efficacy for killing bacteria within colonies. Of the six bactericidal antibiotics considered here, ciprofloxacin was most effective, followed by gentamicin. After 24 hours of exposure, these two antibiotics were able the clear the bacterial population by more than 3 orders of magnitude. The physical structure of colonies only provided temporary protection on the cells within colonies, serves a

delay of the killing effects from the antibiotics. Of the beta-lactam antibiotics, ampicillin was more effective in killing *S. aureus* in colonies than oxacillin, which even failed to inhibit the growth of the older colonies initiated with 10^4 cells per filter. In our experiments, daptomycin, which is considered bactericidal [98, 124, 125, 126], was no more capable of killing *S. aureus* in colonies than the antibiotics that are deemed bacteriostatic, tetracycline, erythromycin and linezolid. Indeed, this cyclic peptide was less effective in preventing the proliferation of *S. aureus* in more mature (48 hour) colonies than these bacteriostatic drugs. Vancomycin, which is commonly employed for treating methicillin resistant *S. aureus* [100, 102, 123, 125, 127], was virtually ineffective for either preventing the replication of or killing *S. aureus* Newman in colonies.

The preceding conclusions about the relative efficacy of the different antibiotics for treating *S. aureus* as colonies is based on a common dose of 10X MIC of these drugs with 24 and 48-hour inoculum densities respectively of $\sim 2 \times 10^7$ and $\sim 2 \times 10^8$ cells per ml for the experiments with 50 colonies and $\sim 3 \times 10^8$ and $\sim 9 \times 10^8$ the experiments initiated with 10^4 colonies per filter. These densities are substantially greater than the recommended 5×10^5 cells per ml for estimating MICs [115] by serial dilution. To some extent the differences in relative efficacy of the bactericidal antibiotics to kill *S. aureus* in colonies may be attributed to a density (inoculum) effect [118]. On the other hand, we dont see the utility of reducing the density of cells treated to make these drugs more effective in this experimental system. From a clinical perspective, concern is to treat established infections the densities of which are likely greater than the 5×10^5 [128, 129].

What about increasing the dose of the antibiotics that were ineffective for treating colonies in these experiments? We have explored this possibility with 40XMIC of oxacillin and vancomycin. The results of these experiments suggest that even at these high concentrations, these antibiotics are ineffective for treating *S. aureus* Newman

in colonies (Fig. A.1).

On first consideration it may seem that the relative inefficacy of vancomycin, oxacillin and daptomycin to kill or prevent the replication of *S. aureus* in colonies may reflect the inability of these drugs to diffuse through the membrane on which the colonies are growing and then through the colonies. We do not believe this is the case for oxacillin or vancomycin, although it is known that to some extent biofilms reduce the rate of diffusion of antibiotics[112, 121, 122, 130, 131]. In our experiments, however, the time of exposure to these drugs was relatively long, 24 hours. We expect that the diffusion effect would be small. Based on what is known about the diffusion rates of these drugs in Staphylococcus in biofilms it seems reasonable to assume the bacteria within these colonies would have been exposed to substantial concentrations of these drugs [121, 122, 131]. Moreover, the cells dispersed from colonies before treatment with these drugs were no more susceptible than those in intact colonies, even though the bacteria were in liquid and confronted with the same concentration of these antibiotics (Fig. A.1). We suggest the primary reason for the relative inability of these antibiotics to kill *S. aureus* in colonies can be attributed to the density and physiological state of the bacteria, rather than the structure of the colonies. In colonies grown on surfaces, it was reported that only the cells on the bottom and the edge of a colony are growing [132, 133], and therefore only these cells will be targeted by the bactericidal antibiotics. On the other hand, the bacteriostatic antibiotics themselves often decelerate the bacterial metabolism rate [134], their efficacy should depend weaker on the physiological states of the cells than bactericidal ones. However, it is still intriguing that the three bacteriostatic antibiotics studied here, tetracycline, erythromycin and linezolid, managed to inhibit the colony growth in all colonies cultures. This effect is very important to support immune system to fight with the bacterial infections *in vivo*.

One possible explanation for why daptomycin is not effective in colonies but is in

liquid is that its mode of action is thwarted by the structure of the colonies. It has been proposed that daptomycin operates by depolarizing the cell membrane which results in leakage of ions [101, 100, 102, 121]. If, however, the cells are within colonies the ions lost by individual cells would remain in the collective and thereby shared by all in this community.

CHAPTER IV

EXPERIMENTAL STUDY AND MODELING OF THE POPULATION DYNAMICS OF NUTRIENT-LIMITED THREE-DIMENSIONAL BACTERIAL COLONY GROWTH

(This chapter is based on "Shao, X., Mugler, A., Kim, J., Jeong, H. J., Levin, B., & Nemenman, I. (2016). Growth of bacteria in 3-d colonies. *arXiv preprint arXiv:1605.01098*".)

4.1 Introduction

From the previous study in Chapter 3, the pharmacodynamics of bacterial colonies on surfaces is affected majorly by two aspects: the cell density in total and the physiological states of the cells. How many cells in the population were deviding and how many were not? How do antibiotic molecule diffuse in the system? These questions related to the population dynamics of bacterial cells have been extensively studied as planktonic cells in well-agitated liquid culture where cells have equal access to nutrients, signaling molecules, and toxins and to each other. This continuous mass culture is convenient for both experimentalists and theoreticians. In 1949, Jacques Monod developed a model for bacterial growth in liquid culture [99], where cells and nutrient molecules are homogeneously distributed.

To grow and divide, cells consume nutrients and convert them to new cell mass. In Monod's model, when nutrients are abundant, a given cell divides at a constant rate, leading to exponential growth of the total cell population. As nutrients become

depleted, this growth slows. When all nutrients are consumed, the population saturates. This process has been well studied in well-mixed liquid media, where cell densities and nutrient concentrations are uniform in space.

However, bacterial cells in the real world do not live in well-mixed liquid environments. Often cells are relatively fixed in place, such that growth and division gives rise to a dense, expanding colony. Population growth in a colony differs physically from population growth in liquid in two important ways: (i) nutrient consumption is limited by diffusion of nutrient molecules to the colony, and (ii) cells at different colony depths may have unequal access to nutrients. Here we focus on the first feature only. Thus we ask: how is growth in a colony altered by nutrient diffusion, as compared to growth in liquid?

There have been abundant number of diffusion models for bacterial growth on surfaces, such as 2-d colonies and biofilms[35, 56, 135, 46, 44]. Complex heterogeneity was considered in these mathematical models such as different diffusion coefficients for every chemical, asymmetric liquid flow. These models carefully depict the heterogeneous distribution of the cellular physiological states in colonies and biofilms, as well as a landscape of nutrient consumption. However, diffusion in one or two dimensions is different from three, making it easier to form diffusion-limited fingers [136, 137, 138].

In 3-d, work has been done to understand nutrient shielding of the interior of a colony by the microbes on the surface, treating them as individual agents [139]. However, we are not aware of 3-d models of colony growth that account for the spatially varying density of nutrients and bacteria, explain the observed experimental phenomenology of bacterial growth in such colonies, and do so in a coarse-grained (PDE) Monod-style fashion, without modeling individual bacteria.

In this chapter, we developed such a minimal model for the growth of *E. coli* colonies embedded in 3-d soft agar and validate it experimentally. The growth rate

heterogeneity only comes from the non-uniform nutrient distribution produced self-consistently by interactions between the bacteria and the nutrient, but we do not assume any heterogeneities beyond this. We neglect cell motility and all mechanical stresses, and we assume that the colony is essentially unconstrained by the soft agar and is free to expand. Our joint theoretical-experimental approach reveals several surprising features of 3-d colony growth, including that bacterial colonies in soft agar are extremely loosely packed with viable cells, and that bacteria grow to larger numbers in colonies than in liquid given the same amount of nutrient. Future studies can use our model as a baseline description of 3-d colony growth, deviations from which can identify emergence of additional phenotypic heterogeneities in the colony.

4.2 Materials and Methods

4.2.1 Bacteria

Escherichia coli Lenski 1976 was used in our study. It is derived from B6 strain described in [140].

4.2.2 Medium

Overnight cultures of *Escherichia coli* Lenski 1976 grew in LB broth (Lysogeny Broth (LB), Becton Diskinson (Franklin Lakes, NJ, USA), well-agitated at 37°C.

Liquid culture was supplemented with Davis Minimal (DM) salts and 0.2mg/ml glucose as the only carbon source. Cells from overnight culture were diluted in saline water and inoculated in DM liquid culture. Sampling was done by series dilution and plating on LB agar Petri dishes.

Colony culture. A schematic protocol is shown in Fig. 4.1a. Colonies were embeded in 0.35% of bacto agar with DM and 0.2mg/ml glucose as the only carbon source. The soft agar were melted in microwave and cooled down before inoculation. After inoculating with cells and before hardening, the melted soft agar culture were aliquoted in to Costar Macrotiter 6-well plates, 3ml in each well (Fig. 4.1b) . Plates

were covered and set in a tray with distilled water to preventing the agar culture from drying. To sample soft agar culture, 3-6 wells of culture were sacrificed at each time point. Soft agar in each well was disrupted and transferred into saline water using long transfer pipette. Vortexing and short sonication was used to further disperse the cells in saline. At last the saline water with cells was sampled by serial dilution and plating on LB agar Petri dishes.

Inoculum: both liquid culture and colony culture were inoculated with 50 cells/ml, unless otherwise noted. Saturation calibration was done(Fig. 4.6) to confirm that 50 colonies/ml is enough for colony cultures to deplete all nutrient while the distance between colonies was large enough to be considered as single colonies within our model.

4.2.3 Imaging

Fluorescent dyes. The dead cells are tagged with Propidium Iodide (PI). Cell membrane was tagged with WGA350 (Wheat Germ Agglutinin, Alexa Fluor 350 Conjugate), including live and dead cells [141, 142]. Both dyes are generous gift from Dr Minsu Kim's lab, originally purchased from Thermo Fisher Science. The working concentration of PI was 4 μM/ml. The working concetraion of WGA350 was 10 μg/ml.

*Cell size measurement.*To measure the cell sizes in liquid cultures at a certain time point, 5 ml of the experiment culture was centrifuged at 4k rpm for 4 min. Certain amount of the supernant was disposed so that the cell density of the resuspension of the rest culture can reach at least 10^7 cells/ml. For colony cultures, centrifuge would not separate the agar and cell. Disperse the colony culture and directly sample from the mixture. In order to have enough cells per slide to image, the 6-hour old cultures were inoculated with 10^6 cells/ml. The 14-hour old cultures were inoculated with 1000 cells/ml. The older cultures were all inoculated with 50 cells/ml.

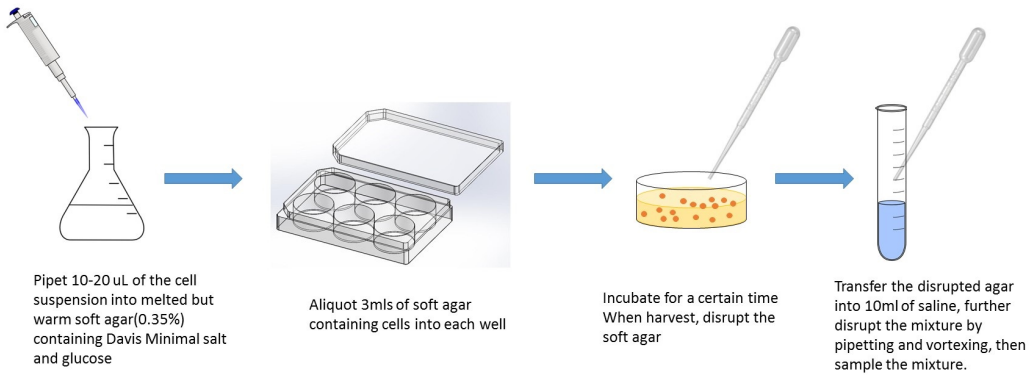

(a)

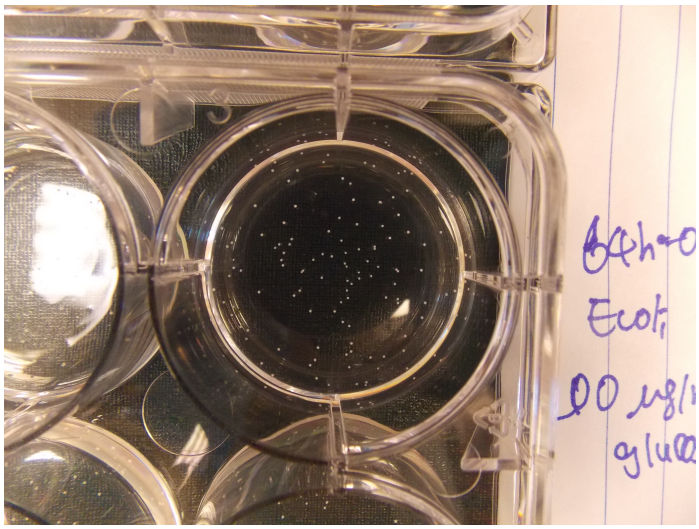

(b)

Figure 4.1: **Experimental setup of the growth and harvest of colony cultures in soft agar.** (a) Illustration of the step protocol of initiating and sampling the colony cultures in soft agar. (b) An expample of colony culture with visible colonies in soft agar in one well of a 6-well macrotiter plate. This colony culture was incubated for 64 hours when pictured. Colonies distributed randomly through out the soft agar and distanced from each other. The shape of the colonies is approximately spherical.

Preparation of chambered coverglasses. In order to observe 3-d colonies using inverted confocal microscope, colony cultures were incubated in Nunc^{TM} Lab-TeK^{TM} II Chambered Coverglass. 230 μl of soft agar containing cells and dyes were aliquoted into each well of 8-well chambered coverglasses. 560 μl if using 4-well. The inoculum size was 5000 cells/ml. The initial glucose concentration was 0.2mg/ml. To prevent the agar from drying after long term incubation, the chambers were wrapped with

parafilms.

Microscopy Confocal imaging. Bacterial colonies in chambered coverglasses were imaged at Integrated Cellular Imaging Core, Emory University, using Leica (Wetzlar, Germany) TCS SP8 inverted confocal microscope with live-cell chamber at 60x (HC PL APO 63x/1.40 oil CS2 WD 0.14 mm),

4.2.4 Image analysis

The images obtained from the confocal microscope were processed using ImageJ (National Institutes of Health, Bethesda, MD). The measurements of dead cells were output by the 3D Objects Counter [143]. These measurements were further analyzed using MatLab.

4.2.5 Numerical solution of the model

The well-mixed Monod model, Eqs. (4.1), (4.2), was solve using `ode15s` MatLab routine. To solve the growth equations Eqs. (4.3)-(4.5) numerically, we rewrote the equations in spherically symmetric coordinates, and then discretize the space into concentric shells so that the partial differential equations become sets of coupled ordinary differential equations describing dynamics within each shell. These were then solved again using Matlab's `ode15s`, with an additional constraint that the radius expands at every time step in such a manner to enforce a constant cell packing density through the colony, as in Eq. (4.5), at every time step. But we did not shrink the inner shells when the cells in them started dying. The total number of cells, including live and dead, is used to calculate the radius of the colony at each time step. Since the soft agar should be so soft that the cells encounter no mechanical confinement and can push out the space freely, it is reasonable to assume a constant cell packing density and that the colony radius expand continuously when cells divide.

4.2.6 Model fitting and confidence intervals estimation

We first fitted the five parameters of the Monod model for the growth in the liquid culture, Eqs. (4.1), (4.2). For this we defined the loss function $\mathcal{L} = \sum_i (N_i - N(t_i; g_{\max}, m, K, \tau_{\rm lag}, a_{\rm l}))^2$, where N_i was the population size (in CFUs/ml) in the i'th measurement, and $N(t_i; g_{\max}, m, K, \tau_{\rm lag}, a_{\rm l})$ was the model prediction for the same time and for given parameter values. Note that we did not average measurements at the same t, but incorporated all individual observations into the loss function, cf. Fig. 4.5. We optimized $\mathcal{L}$ over the five parameters using MatLab's `fmincon`. For K and m, which are small and have large uncertainties, we optimized w. r. t. their logarithms, thus enforcing their positivity (the other parameters were sufficiently constrained by data away from zero even without this reparameterization). The optimization was performed with ten different random initial conditions for the parameters, and the best values from among all the runs were chosen, resulting in the best-fit parameters $\bar{g}_{\max}, \bar{m}, \bar{K}, \bar{\tau}_{\rm l}, \bar{a}_{\rm l}$, which we report in Tbl. 4.

To estimate the confidence intervals for these inferences, we bootstrapped the data 1000 times [144]. When re-sampling with replacements for bootstrapping, we resampled separately from the exponential growth region ($t \leq 22$ hrs) and the saturated region ($t > 22$ hrs), so that the number of data points in each of the regions was fixed in all resampled datasets. We refitted the five growth parameters for each of the resampled data sets. The middle 80% of the best-fit parameter realizations are reported in Tbl. 4 as confidence intervals, and the covariances among the bootstrapped best-fit values are reported in Tbl. 6. Since the sensitivities to the parameters vary widely, and $\mathcal{L}$ near its minimum is badly approximated by a quadratic form, we additionally report confidence intervals directly on the model predictions, rather than just the parameters. For this, for each of the 1000 resampled datasets, we calculated the population growth with the best-fit parameters, and the middle 80% of these growth curves are shown as the colored band in Fig. 4.5 (top).

For fitting the 3-d growth model, Eqs. (4.3)-(4.5), we write the loss function $\mathcal{L} = \sum_i (N_i - N(t_i; \bar{g}_{\max}, \bar{m}, \bar{K}, \bar{\tau}_l, a_c, D, \mu))^2$. This is minimized as above over a_c, D, μ, with the first four parameters inherited from the optimizations for liquid data. Results of the optimization are shown in Fig. 4.5 (bottom). To establish confidence intervals, we bootstrap the entire analysis pipeline 30 times (the number is limited since parameter optimizations for PDEs describing the nutrient dynamics are computationally costly), resampling both the liquid and the 3-d colony data. While resampling the colony data, we keep the number of data points in each of the three regions constant (exponential, $t < 24$, diffusion-limited, $24 \leq t < 48$, and saturated, $t \geq 48$). Confidence intervals on parameters and model predictions in Fig. 4.5 (bottom) and Fig. 4.6 are then done as explained above. We use the same bootstrapped data sets to estimate the covariances and correlations of the parameters (Table. 6). These are evaluated as empirical covariances and correlation coefficients of the best-fit values for the bootstrapped data sets.

4.3 Results

4.3.1 The experimental results of bacterial growth in liquid cultures and as 3-d colonies

To quantitatively control the growth of bacterial population, we used *Escherichia coli* cells growing in DM liquid broth or embedded in DM soft agar. The only carbon source was glucose, of which the initial concentration was 0.2 mg/ml. Unless mentioned otherwise, 3-d colonies are grown in 3 ml of soft agar, inoculated with approximately 50 colonies/ml, so that each colony has an access to a nutrient subvolume of $v \sim 1/50$ ml, or an effective sphere of nutrient with radius $R = (3v/4\pi)^{1/3} \approx 1.7$ mm (Fig. 4.1b). The growth curves, $N(t)$, for liquid cultures and colony cultures were measured at various time points by harvesting, diluting, and plating cells, and then counting the number of resulting colonies that form on a plate (see *Methods* for details). By this mean, $N(t)$ represents time-dependent measurements of the colony

forming units(CFUs) per ml. Measurements of $N(t)$ in the experiments are shown in Fig. 4.2 (experiment data points). After the lag phase, the population in the liquid culture rises exponentially, and then abruptly saturates and starts decaying at a very slow rate as the cells are dying. On colony growth curve, the labg phase and the exponential phase before 22 hours are overlapping with that of liquid culture. In contrast of an abrupt stop in growth of liquid culture, in 3-d colonies, the exponential growth and the saturation are separated by a gradual, sub-exponential growth regime. We hypothesize that this is because the growth here is limited by the speed with which diffusion brings nutrients from the edges of the nutrient subvolume to its center, where the bacteria metabolize them. Another surprising result is that the maximum population size for the colonies is larger than that for the liquid, which indicates the same amount of nutrients yields more bacteria in the physically structured environment. To understand these findings quantitatively, we now develop the minimal mathematical model capable of explaining them.

4.3.2 Minimal model of resource-limited bacterial growth

The growth model for bacterial population in liquid cultures has been maturely developed. Here we inherited the linear growth model built by Monod in 1949 [99], where all cells grow at the same rate and the rate depends on the current density as $g(\rho) = g_{\max}\rho/(\rho + K)$. Here $g_{\max}$ is the maximum growth rate that a cell can reach, and K is the half-saturation constant, so that the growth rate is half of the maximum when the nutrient concentration is $\rho = K$. Thus we have the cell density $n = N/v$ that obeys

$$\frac{dn}{dt} = n\,\Theta(t - \tau_{\text{lag}})\frac{g_{\max}\,\rho}{\rho + K} - nm, \tag{4.1}$$

$$\frac{d\rho}{dt} = -\frac{1}{a_{\text{l}}}n\,\Theta(t - \tau_{\text{lag}})\frac{g_{\max}\,\rho}{\rho + K}. \tag{4.2}$$

Here v is the volume of the liquid where the culture grows, and a_{l} is the liquid *yield*, which measures the number of bacteria produced by per microgram of glucose.

Further, $\Theta(t-\tau_{\rm lag})$ is the Heaviside Θ-function, which is equal to zero for $t<\tau_{\rm lag}$, and to unity otherwise. It represents the lag phase before the growth starts after a transfer to a new environment. Note that Eqs. (4.1) and (4.2) differ slightly from the standard Monod model. Specifically, we added a small constant death rate m to account for the decrease of the population in the liquid culture after the saturation (Fig. 4.2). Thus the population has a zero net growth at a critical nutrient density of $\rho_{\rm m}=mK/(g_{\rm max}-m)$, which represents the minimum nutrient concentration needed to sustain life without growth [145, 146].

In our minimal model of 3-d colony growth, we assume that the bacterial cells within a colony are genetically identical, but depending on their position, vary in their access to the diffusing carbon source. Therefore the growth rate of every individual cell still obeys the Monod equation. The difference is that ρ is no longer averaged over the whole system, but varies locally, denoted as $\rho(x,y,z)$.

The turgor pressure in *Escherichia coli* was estimated at about 1 to 3 atm [141, 147, 148]. In addition, there is no limitation on the migration or the swarming of *Escherichia coli* cells on soft agar plates if the concentration of agar is below 0.4% [149, 150]. Therefore it is reasonable to assume that the cells expands freely in the 0.35% soft agar, with no feeling of physical obstruct. As the cells divide, the colony expands symmetrically as a sphere. New daughter cells push their way out freely, keeping a constant cell density per volume of the space occupied by the colony. This leads to the following equations for the spherically-symmetric local number density of cells $n(r,t)$ and nutrient concentration $\rho(r,t)$:

$$\frac{\partial n(r,t)}{\partial t}=n(r,t)\,\left[\Theta(t-\tau_{\rm lag})\frac{g_{\rm max}\,\rho(r,t)}{\rho(r,t)+K}-m\right], \tag{4.3}$$

$$\frac{\partial \rho(r,t)}{\partial t}=D\nabla^2\rho-\frac{1}{a_{\rm c}}n(r,t)\,\Theta(t-\tau_{\rm lag})\frac{g_{\rm max}\,\rho(r,t)}{\rho(r,t)+K}, \tag{4.4}$$

with the initial uniform spatial concentration of the nutrient $\rho(r,0)=\rho_0$ at time $t=0$, and a single bacterium starting at $r=0$. In these equations, D is the nutrient

(glucose) diffusion coefficient. Further, we allow for the yield in the colony $a_{\rm c}$ to be different from the liquid yield $a_{\rm l}$ to account for the different saturation values in Fig. 4.2, as further discussed below. Importantly, since the agar is more than 99% liquid, the four other growth parameters $g_{\max}$, K, $\tau_{\rm lag}$, and m are taken to be the same in both media.

To keep the cellular packing density μ as a constant inside a colony, the radius of the colony must increase when cells devide. We require that the overall increase in cell number leads to the proportionate growth of the colony radius $r_{\rm c}$, so that $N \equiv 4\pi \int dr\, r^2 n(r,t) = (4/3)\pi r_{\rm c}^3 \mu$. Thus at each point in time, we impose the condition that

$$n(r,t) = \begin{cases} \mu, & 0 < r \le r_{\rm c} = (3N/4\pi\mu)^{1/3}, \\ 0, & r_{\rm c} < r \le R, \end{cases} \tag{4.5}$$

Accoding to experimental results, there should be four regimes on the growth curve of a 3-d bacterial colony: lag regime, exponential regime, diffusion-limited regime and the slow death regime. To illustrate the behavior of this 3-d model of bacterial growth as colonies, we plot numerical solutions of Eqs. (4.3)-(4.5) for different values of the nutrient diffusion coefficient in Fig. 4.4 (A). Especially at small D, two different growth regimes are clearly visible after the lag but before the ultimate saturation and the slow cell death. The first is the fast *exponential growth* based on local, immediately accessible resources. This regime is indistinguishable from the growth in liquid. When the local nutrients are depleted at a certain time τ_1 following the start of the growth at $\tau_{\rm lag}$, new nutrients must be brought from afar by diffusion. This is slow, resulting in a slower *diffusion-limited growth* regime. Here the overall colony growth rate is an average over cells growing at different rates due to different concentrations of the locally accessible nutrient. Our simulations suggest that, in this regime, the nutrient concentration at the colony edge decays exponentially fast, in agreement with Ref. [139], cf. Fig. 4.4 (B). The nutrient penetration depth is only

a few μm, or a few cell layers. Therefore, in the diffusion-limited regime, there are, essentially, no nutrients deep inside a colony, and only cells at the periphery can grow. In the absence of resource storage [151], nutrient sharing from the outer cells, or cannibalism (we model none of these), interior cells would not grow at all and will eventually die. The diffusion-limited growth regime finally ends with *saturation* and *slow death* when most of the nutrients in the accessible subvolume are depleted at time τ_2 after $\tau_{\rm lag}$. The onset of the saturation takes longer than in liquid since small (but larger than $\rho_{\rm m}$) amounts of the nutrient linger at the far edges of the nutrient subvolume for a long time.

Analytical expressions for the time when the exponential regime transit to diffusion-limited regime τ_1, the time when diffusion-limited regime transit to the last regime τ_2, and the growth dynamics can be obtained from the following arguments. First, during the exponential growth regime, the population grows as $N \sim e^{g_{\max}t}$. This requires the nutrient mass in the amount of $e^{g_{\max}t}/a_{\rm c}$, which must come from the volume immediately accessible by diffusion, equal to $\sim \rho_0(\sqrt{Dt})^3$. Equating the two expressions gives, to the leading order, $\tau_1 \sim g_{\max}^{-1}\log[\rho_0 a_{\rm c}(D/g_{\max})^{3/2}]$. When local resources are exhausted, growth is limited by nutrients diffusing in from the volume $\sim(\sqrt{Dt})^3$. However, because the encounter probability for a 3-d random walk is less than one [152], most of the nutrient molecules coming from afar will not be immediately absorbed. In fact, since the box-counting dimension of a diffusive process is two, only $\sim \rho_0(\sqrt{Dt})^2 r_{\rm c}$ amount of nutrient molecules will be captured in time t, resulting in $N \sim \rho_0 D t r_{\rm c} a_{\rm c}$. On the other hand, the radius of the colony grows as $r_{\rm c} = (3/4\pi)^{1/3}(N/\mu)^{1/3}$. Combining these expressions gives $N \sim [(a_{\rm c}\rho_0 D)^3/\mu]^{1/2} t^{3/2}$ in the diffusion-limited regime. Finally, the total amount of nutrients available to the colony is $\sim \rho_0 R^3$, and so the diffusion-limited growth will saturate, and the population will start decreasing at the rate of m when the colony grows to $N \sim a_{\rm c}\rho_0 R^3$,

which occurs at $\tau_2 \sim (\mu/a_c\rho_0)^{1/3}R^2/D$. Altogether, we find

$$N \sim \begin{cases} \text{const}, & t < \tau_{\text{lag}}, \\ e^{g_{\max}t}, & t - \tau_{\text{lag}} \ll \tau_1 \sim \frac{\log\left[\rho_0 a_c \left(\frac{D}{g_{\max}}\right)^{3/2}\right]}{g_{\max}}, \\ \left[\frac{(a_c\rho_0 D)^3}{\mu}\right]^{\frac{1}{2}} t^{3/2}, & \tau_1 \ll t - \tau_{\text{lag}} \ll \tau_2 \sim \left(\frac{\mu}{a_c\rho_0}\right)^{\frac{1}{3}} \frac{R^2}{D}, \\ a_c\rho_0 R^3 e^{-mt}, & \tau_2 \ll t - \tau_{\text{lag}}, \end{cases} \tag{4.6}$$

These analytical estimates are supported by the numerical solutions in Fig. 4.4(A). The transition time τ_{lag}, τ_1 and τ_2 are calculated according to the parameters of the purple curve. We specifically plotted the green growth curve with an unrealistically low value of diffusion coefficient in order to present a wide and clear range of diffusion limited regime. The dash line of $t^{3/2}$ goes parallel along the green curve.

We note that in one or two dimensions, the diffusion limited growth would scale as $N \propto t^{d/2}$ for dimension d, independently of the (small) colony radius, or even for a point colony, since the random walk encounter probability there is one [152]. In contrast, our three-dimensional result depends critically on knowing how the radius of the colony scales with the number of growing bacteria. In particular, here we cannot model the colony as a point-like object. Thus the exponent of the power law scaling is not universal in 3-d, and it may change for heterogeneous colonies with varying cell size and cell density.

4.3.3 Parameter optimization of the minimal model of bacterial growth

To determine the extent to which our minimal model accounts for the dynamics of growth of bacteria in colonies, we fit the model to data using nonlinear least squares fitting, similar to the liquid case. We keep the parameters a_l, K, $g_{\max}$, m, and τ_{lag} equal to the values inferred for liquid, and only optimize D, μ, and a_c for the 3-d culture data. See *Materials and Methods* for the details of the fits, including estimation of the prediction uncertainty using bootstrapping. Table 4 shows fitted parameter values with the corresponding nominal values from the literature. The

fitted parameters are consistent with the nominal values where the latter are known. Further, the best fit curve shows an excellent agreement with data (cf. Fig. 4.2, red), and the prediction confidence bands are very narrow (cf. Fig. 4.5). This suggests that nutrient diffusion and the ensuing geometric heterogeneity of growth are sufficient to explain the population dynamics of these *E. coli* colonies in 3-d at our experimental precision, and consideration of additional phenotypic inhomogeneities is not needed.

Our analysis also provides estimates of two previously unknown parameters, μ (packing density) and a_c (yield in 3-d colonies). The inferred packing density is $\mu = 3.0 \cdot 10^{-2}$ CFUs/μm^3, with the 80% confidence interval of $[1.7, 4.2] \cdot 10^{-2}$ CFUs/μm^3 . Since an *E. coli* cell has a volume of between 0.5 and 2 μm^3 [52, 53], this suggests that only about $\sim 3\%$ of all space in a colony is occupied by viable cells. This is a surprising finding, and it requires an independent corroboration. Towards this end, we measure radii of large colonies and calculate their packing densities by diving colony volumes by the average CFUs per colony. This gives $\mu = 1.5 \pm 0.08 \times 10^{-2}$ CFUs/μm^3, consistent with our estimation of μ from the fitted growth model. In other words, in our experiments, viable *E. coli* cells like to keep their distance from each other.

The second inferred parameter is a_c. We find that the yield as measured by the ratio of the CFUs estimated stationary phase density and the quantity of glucose in 3-d is 2 to 3 times higher than that in liquid culture, $a_c > a_l$ (cf. Table 4). This implies that, at saturation, colonies produce more CFUs than liquid cultures, which is directly apparent from Fig. 4.2. This is a surprising result, since in the colony the bacteria grow more slowly and there is more time for cell death. Nonetheless, similar results have been reported for colonies growing on surfaces [54]. Here this effect is likely a direct consequence of the growth dynamics during the diffusion-limited regime. Indeed, *E. coli* cells growing at a rate of > 1 hr^{-1} grow to be 2 to 3 times larger than cells growing at a rate of < 0.1 hr^{-1} [49]. While the diffusion limited

regime lasts only for a few hours (cf. Fig. 4.2), more than 90% of all cells emerge at that time, so that the majority of cells in the colony are smaller than in liquid, yielding more cells from the same nutrient amount.

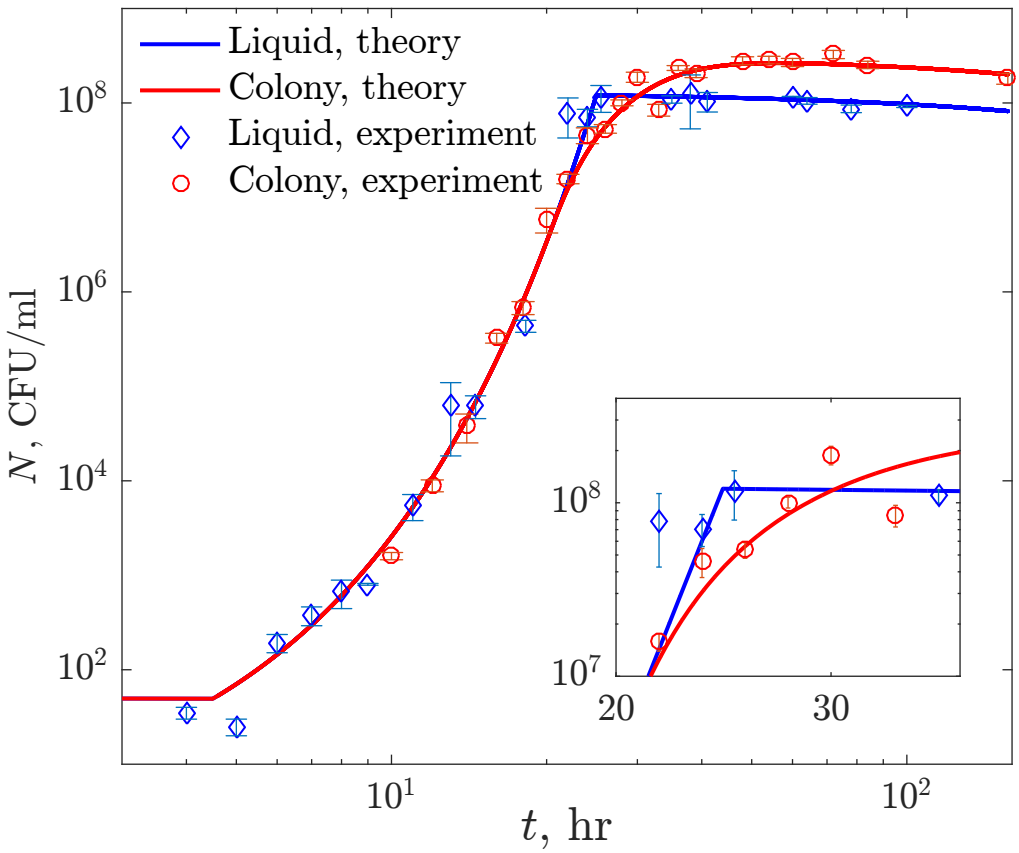

Figure 4.2: ***E. coli* population dynamics.** Experimental data (symbols, error bars are s. e. m.) are compared with the fits of the mathematical model we developed (solid lines). For clarity, uncertainty of the numerical predictions is omitted and is shown instead in Fig. 4.5. Liquid cultures switch abruptly from the exponential growth to the saturation, and then decay slowly. In contrast, 3-d colonies gradually slow down before saturating (see Inset) at a population size larger than in the liquid, and then decay.

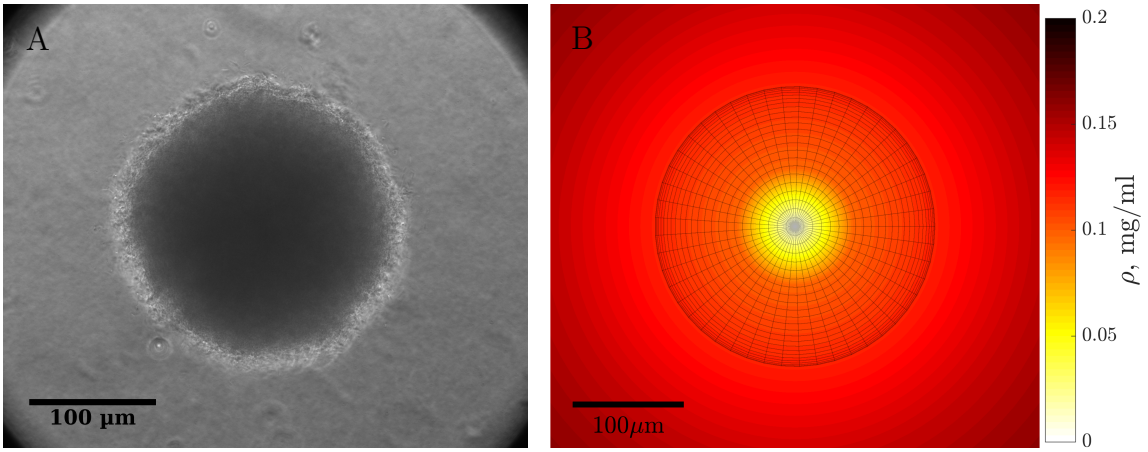

Figure 4.3: **Growing 3-d colony.** (A) Photograph of a representative *E. coli* colony inside 3-d agar at 22 hrs post inoculation. (B) A growing colony at 22 hrs as simulated using our mathematical model. Heatmap shows the spherically symmetric nutrient concentration, and the meshgrid sphere represents the colony. At this time, the nutrient at the center of the colony is fully consumed. Since the growth rate depends on local nutrient concentration, the cells inside of the colony are not growing anymore.

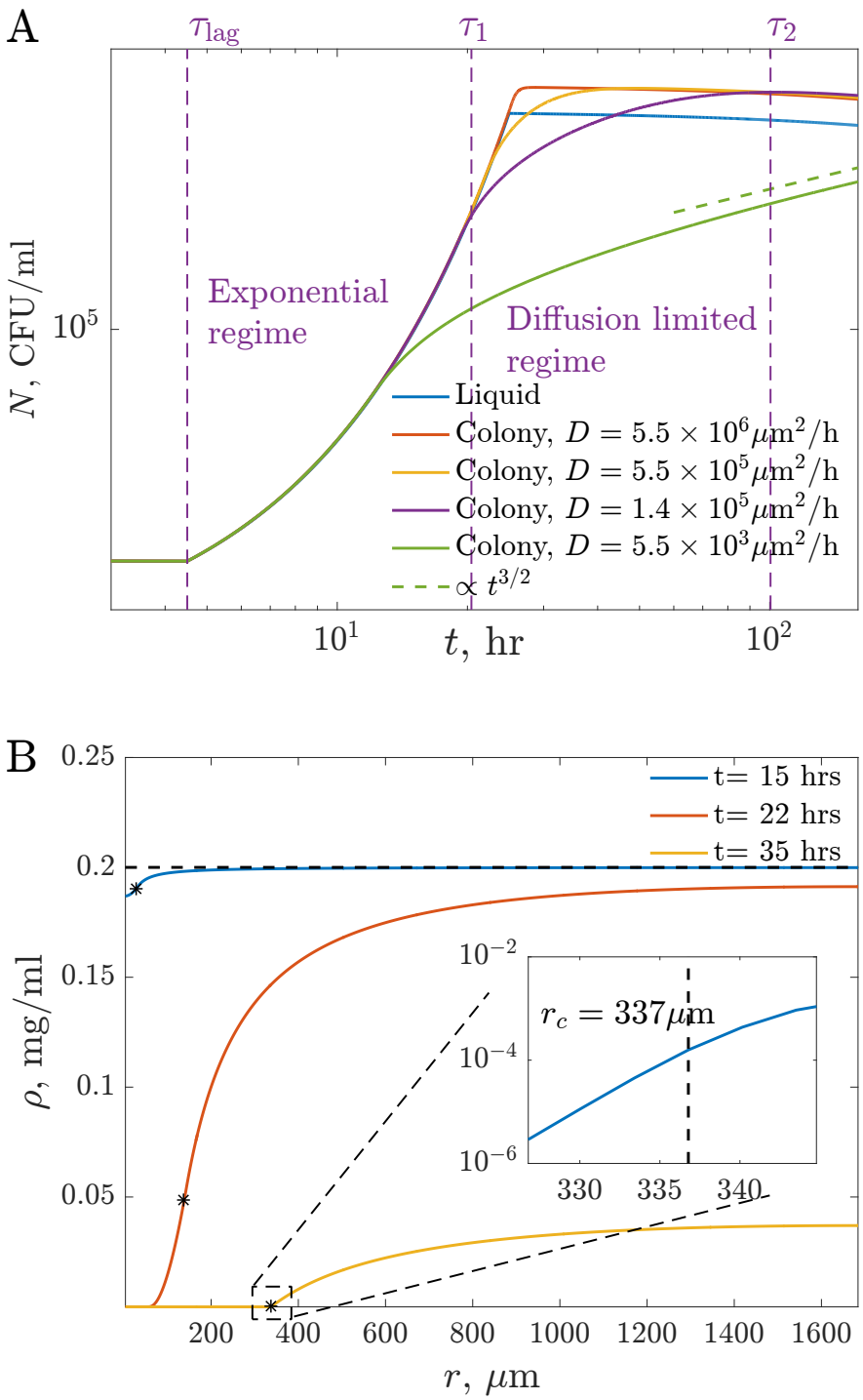

Figure 4.4: **Mathematical model predictions.** (A) Population growth in liquid culture and in 3-d colonies. The growth parameters are chosen as best fit values for our experimental data (see Table. 4), except for D, which we vary to illustrate different growth regimes. The diffusion-limited regime in the limit of small D is consistent with the prediction $N \propto t^{3/2}$. The time scales τ_i are illustrated for $D = 1.4 \times 10^5$ $\mu\text{m}^2/\text{hr}$. (B) Profile of the nutrient concentration in space at different times using the same parameters as above and $D = 5.5 \times 10^5$ $\mu\text{m}^2/\text{h}$, as in Table. 4. The edge of the colony is illustrated by stars on each curve. The inset shows that the concentration decreases exponentially at the colony edge in the diffusion-limited growth regime. The penetration depth is about 3 μm.

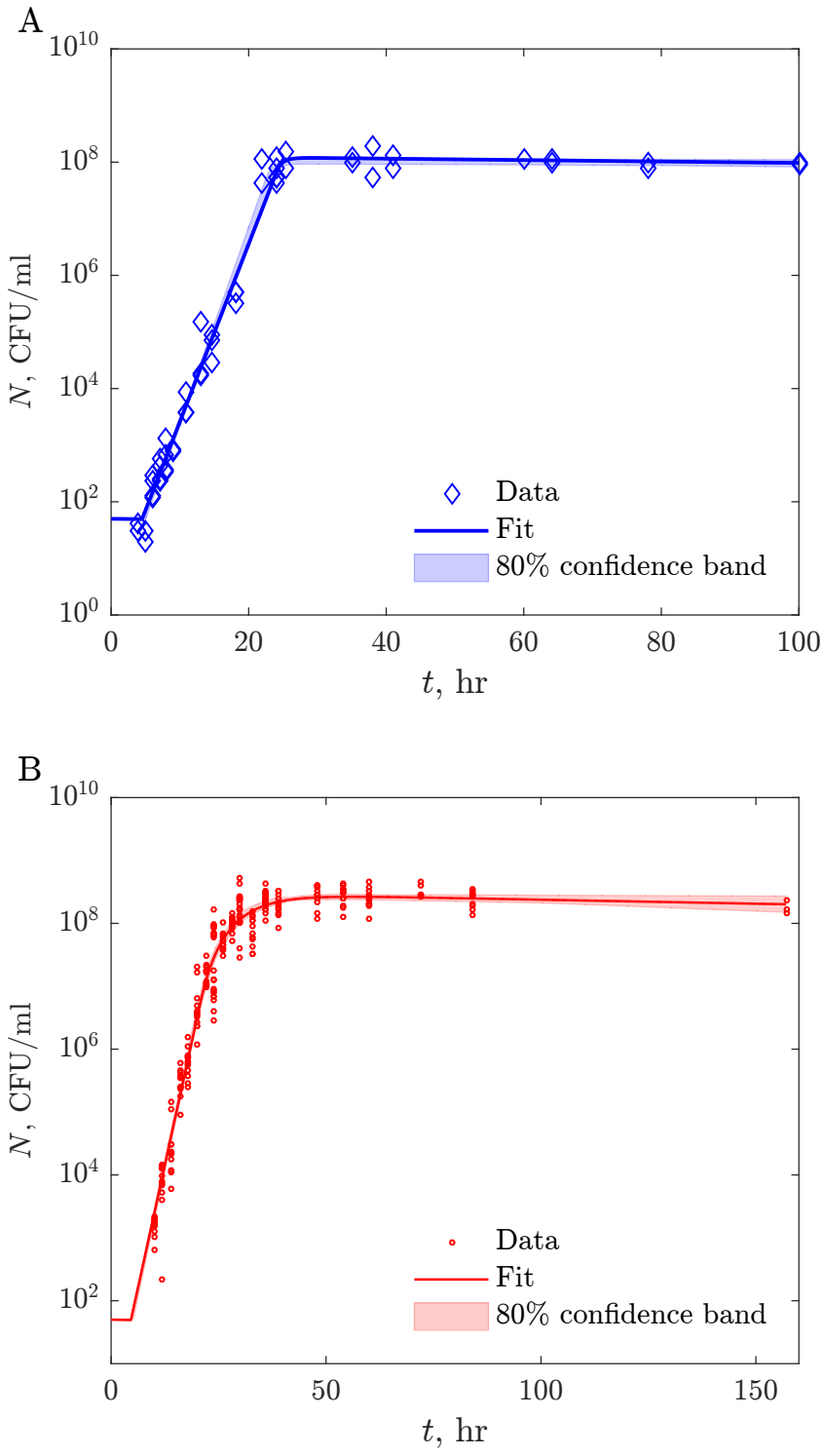

Figure 4.5: **Fitting models to data**. *A*: Liquid growth model (solid blue line) fitted to all of the experimental data we have collected (blue diamonds). 80% confidence intervals around the best-fit predictions are shown by light blue shaded bands (established by bootstrapping, with 1000 resamplings). *B*: same, but for 3-d colony growth. Red circles, solid red line, and light red band correspond to the data, the best fit, and the 80% confidence intervals (from 30 resamplings).

Table 4: **Fitted parameters of the growth models for liquid culture and 3-d colony.**

Name	**Description**	**Literature values**	**References**	**Fitted value**	**80% confidence interval**
$g_{\max}$	maximum growth rate, hr^{-1}	$[0.52, 0.83]$	[52, 153, 154]	0.73	$[0.56, 0.89]$
K	half-saturation constant, μg/L	35	[154]	122	$[19.5, 783]$
a_{l}	yield in liquid, 10^6 CFUs/μg glucose	$[0.5, 1.2]$	[140, 155]	0.61	$[0.54, 0.67]$
τ_{lag}	lag phase duration, hr	$[2, 5]$	[156]	4.5	$[4.3, 4.7]$
m	death rate, hr^{-1}	$[0.0049, 0.018]$	[146, 154]	0.0029	$[7.7 \times 10^{-4}, 0.011]$
a_{c}	yield in 3-d colony, 10^6 CFUs/μg glucose	N/A		1.50	$[1.36, 1.63]$
D	glucose diffusion in 0.35% agar, $\mu\text{m}^2/\text{hr}$	1.8×10^6	[157]	0.55×10^6	$[0.21, 0.89] \times 10^6$
μ	packing density, CFUs/μm^3	N/A		2.98×10^{-2}	$[1.74, 4.22] \times 10^{-2}$

4.3.4 Experimental tests of the model's predictions and observations beyond the model

As an independent test of the developed 3-d growth model, we use it to predict results of experiments distinct from those used for fitting the model. Specifically, we investigate how the population size depends on the density of bacteria used to inoculate the soft agar. At a long measurement time (72 hrs), our model predicts a non-monotonic dependence of the population size on the inoculation density (cf. Fig. 4.6, dashed line). This is because, at very low densities, each colony has access to a large nutrient subvolume, and the colony cannot clear this subvolume by diffusion in just 72 hrs. As a result, at the end of the experiment, there are still nutrients in the media, and the colony does not reach its maximum size. In contrast, at very high inoculating densities, colonies rapidly exhaust their small available nutrient subvolumes, the cell death becomes important throughout much of the experiment duration, and the population is smaller again. Thus the population reaches its maximum at intermediate densities, where these two effects balance. We test this prediction by experimentally measuring population sizes at 72 hrs for *E. coli* growing in soft agar at inoculums varying from 10^1 to 10^5 cells/ml As seen in Fig. 4.6, the experimental data agree with the prediction within errors and, in particular, exhibit the expected non-monotonicity. We emphasize that no additional fitting was done for this figure, and yet the agreement between the experiment and the theory is very good.

Accoding to the experimental data, the yield of glucose in 3-d colonies is 2 to 3 times higher than that in liquid culture and wehave suggested that this is because the cells in liquid cultures are larger than those in 3-d colonies. To verify this hypothesis, we measured the cells sizes of both liquid culture and in 3-d colonies at different time after inoculation. The cell size distribution in liquid culture is shown in Fig. 4.7. The mean cell length at 6 hours post-inoculation was 1.9 ± 0.7 μm. As the cultures grew older, the average cell length increased quickly (Fig. 4.10b). More and longer

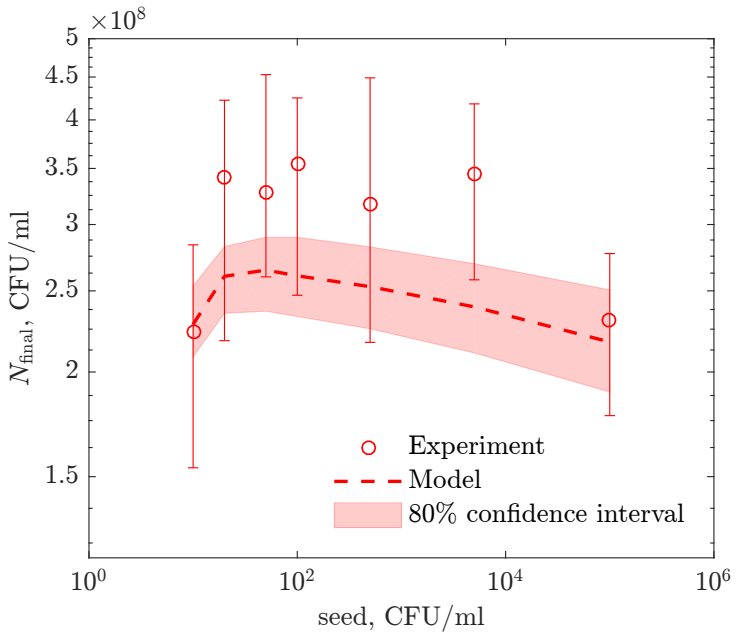

Figure 4.6: **Dependence of the population size on the inoculation density.** Colony cultures inoculated with different cell densities grow to different population sizes. The inoculates are 10, 20, 50, 100, 500, 1×10^3, 5×10^3, and 1×10^5 cells/ml. Circles are experiment data measured at 74 hr post inoculation, and error bars are s. e. m. The best-fit 3-d bacterial growth model reproduces these data within experimental error bars and computational confidence interval, without additional fitting.

filamented cells emerged in the culture. The median cell size, however, fluctuated around 2 μm. The maximum of cell length measured in liquid cultures was nearly 150 μm. If we cut off the filaments with length over 5 μm, the cell size distrubution is much narrower, with a long tail on the right (Fig. 4.8), resulting in a similar shape to those previously described in [50, 51]. Comparing the proportion of cells shorter than 3 μm, the liquid cultures and the colony cultures trend in the opposite directions. As the cultures grew older, the proportion of cells shorter than 3 μm in colonies increased rapidly and saturated near 1. On the other hand, the proportion in liquid cultures decreased and fluctuated near 60% (Fig. 4.10a).

As expected, the cell size in colony cultures was much short than that in liquid culture. Only less than 1% of the sampled cells were longer than 5 μm (Fig. 4.9).

The mean of cell length mildly decreased over time (Fig. 4.10b). The ratio of the mean cell length in the two cultures at different times (Fig. 4.10c) is around 1 before 20 hours and starts to increase after. At 72 hours, the ratio is 3.32 and shows no sign of a plateau. This is consistent with our model that the ratio of cell size in liquid culture to that in 3-d colonies should be 1 during the exponential growth regime, but should increase after the growth in colonies transit to the diffusion limited regime.

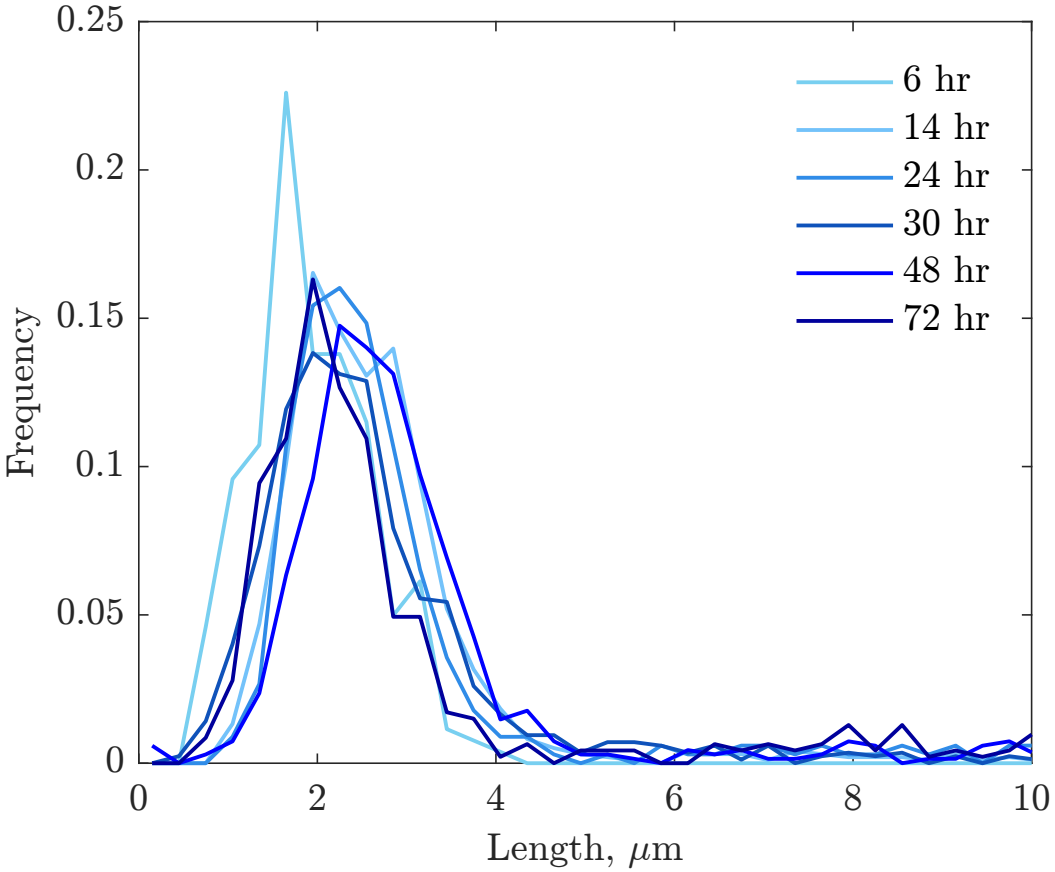

Figure 4.7: **Cell size distribution for liquid cultures.** Cell sizes were measured at 6 hours, 14 hours, 24 hours, 30 hours, 48 hours and 72 hours.

We also look into how the dead cells distributed inside a 3-d colony. Intuitively, the cells that starve the first should die the first. And our model shows that the nutrients are depleted starting from the center of a 3-d colony. Therefore, we expected to see random death throughout the colony when the growth is within the exponential

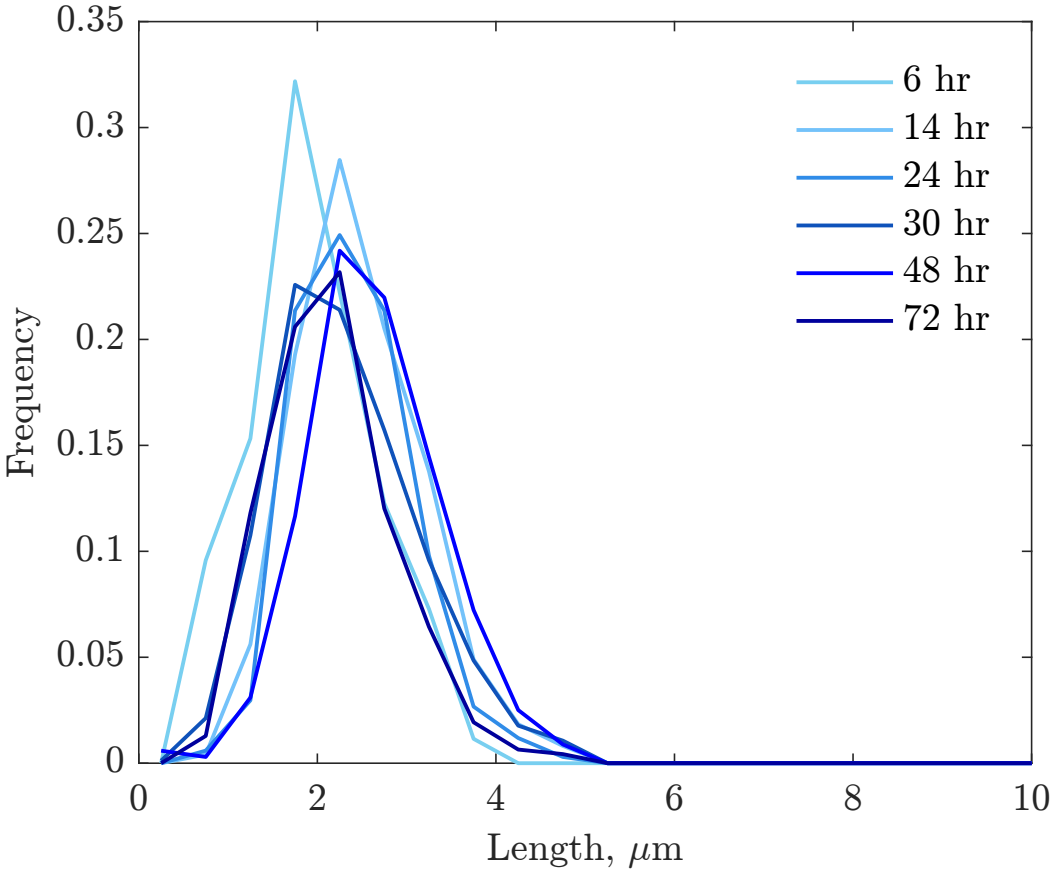

Figure 4.8: **Cell size distribution of short cells (shorter than 5 μm) in liquid cultures.** Cell sizes were measured at 6 hours, 14 hours, 24 hours, 30 hours, 48 hours and 72 hours. All the histograms plot the counts of cells shorter than 5 μm. Longer cells are not included in these plots.

regime, and higher density of dead cells at the center of a colony when the colony is in the late diffusion-limited regime or saturation regime. To verify these predictions, we imaged 3-d colonies at 24 hours, 48 hours and 120 hours of growth with Propidium Iodide (PI), a fluorescent dye that stains only the dead cells, in the agar. We analyze the coordinates of the dead cells tagged with PI and show the densities of dead cells from the periphery towards the center of colonies in Fig. 4.11. At 24 hours, there is no significant trend of decreasing or increasing of the dead cell density, indicating random emergence of the cell death throughout the colonies. At 48 hours and 120 hours, the density of dead cells clearly decreases towards the center of colonies, which

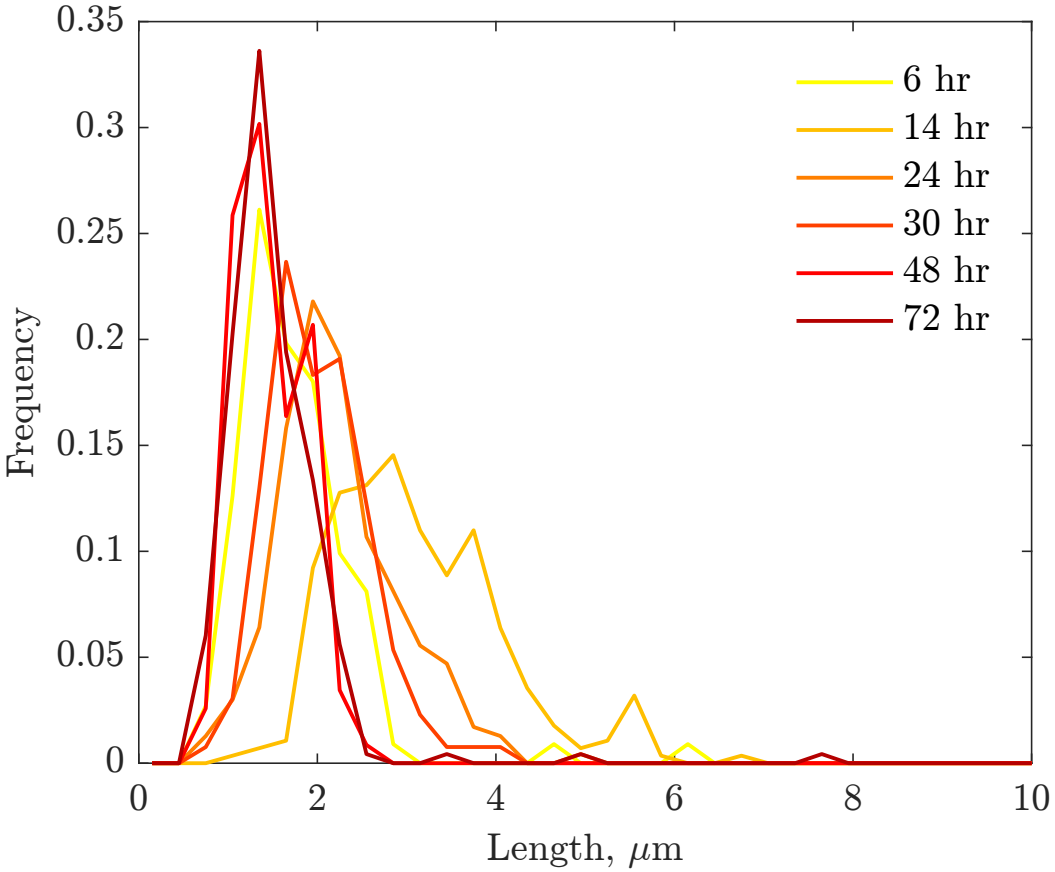

Figure 4.9: **Cell size distribution of colony cultures.** Cells grown in colonies were dispersed into liquid buffer and prepared on glass coverslides in the same way as the cells from liquid culture. Cell sizes at 6 hours, 14 hours, 24 hours, 30 hours, 48 hours and 72 hours.

is opposite of the model prediction.

4.4 Discussion

To our knowledge, the model developed here is the first course-grained, rather than individual-based, model to explicitly study bacterial growth as colonies. We consider this the minimal model because it assumes that the availability of nutrients (a carbon source) is the sole factor determining the rate of cell division within colonies. In reality, the cellular growth, division, and death rates would also depend on cell-to-cell interactions of various sorts, on the enrichment and deterioration of the environment

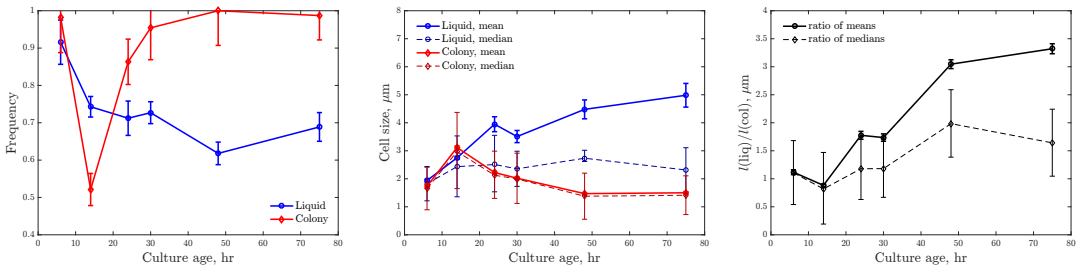

(a) (b) (c)

Figure 4.10: **The comparison of cell sizes in the liquid cultures and colony cultures.** (a) The proportion of cells that were shorter than 5 μm in the bacterial population in liquid cultures and colony cultures. Blue represents liquid cultures. Red represents colony cultures. Error bars are the ratio of the square root of the short cell counts to the total counts. (b) The mean and median cell size in liquid and colony cultures. The blue lines represent liquid cultures. The orange represent colony cultures. Error bars of the means are s. e. m. Error bars of the medians are the 95% confidence intervals of the means. (c) The ratio of cell sizes in liquid cultures to that in colony cultures. The solid line with circles shows the ratio of average cell sizes in liquid cultures to that in colony cultures. The dashed line with diamonds shows the ratio of the median cells sizes in these cultures. Error bars are propagated from the error bars of means and medians.

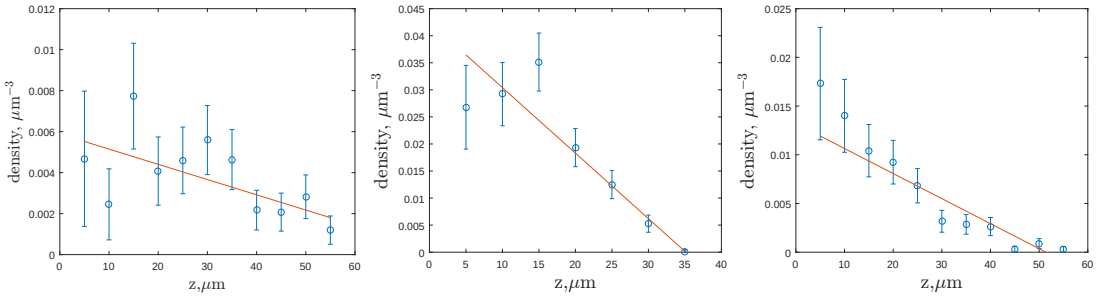

(a) 24-hour-old colony. (b) 48-hour-old colony. (c) 120-hour-old colony.

Figure 4.11: **Dead cell density in 3-d colonies grown for 24, 48, and 120 hours.** Blue circles show the density of dead cells in slices of a colony with depth of 5 μm. The direction of $z-$axis is from the surface towards the center of a colony. Error bars are the square root of the counts in each slice divided by the volume of the slice. Orange lines are regression with weighted least squares.

due to the buildup of secondary metabolites and waste, on cell-environment mechanical interactions, and on diverse cellular phenotypic commitments. The model we developed and experimentally tested here only accounts for the spatial heterogeneity in access to the diffusing nutrient and assumes no such additional effects [158, 159, 151].

Nevertheless, despite these limitations, with only five parameters describing the growth in liquid, and only three additional parameters specific to the 3-d colony growth, this model provides an impressively accurate description of growth of populations of *E. coli* as colonies in soft agar as well as planktonic cells in liquid. Unlike the anticipated and observed nearly precipitous termination of growth in liquid culture as nutrients become depleted, our 3-d model accounts for the experimentally observed gradual reduction in net rate of replication as diffusion of the resource increasingly limits colony growth with time. With no additional fitting, the model also correctly *predicted* the non-monotonic, upside-down U shaped dependence of the population size on the inoculating bacterial density. Moreover, all of the best-fit parameters inferred from the data agreed with prior estimates in the literature, where these are available (see Table 4 and references therein), indicating high-quality fits without overfitting.

Our study has revealed and/or confirmed several intriguing observations about bacteria growing in colonies. First, the growth in colonies yielded substantially greater viable cell densities than obtained in liquid culture with the same concentrations of limiting carbon source. We propose that this is a direct consequence of the diffusion-limited growth, which happens at a slower division rate. In turn, slow division is correlated with smaller size of bacterial cells [49, 50, 51, 52, 53], resulting in more bacteria for the same nutrient amount. This slowing down is very important phenotypically — according to our model, over 90% of all bacteria in the colony are formed at such decreased growth rate, and the yield a_c is an average over yields at different stages of the slowing. We extended our experiments to measure the size of individual cells in liquid culture and in 3-d colonies. The ratio of the mean of the cell length in liquid culture to that in 3-d colonies is consistent with our model.

Our second intriguing observation, which is supported by two independent sets of measurements, is that the packing density inside colonies is very low, $\mu \sim 0.03$

CFUs/μm^3, so that the vast majority of a volume of a colony is not occupied by viable cells. One possibility is that the colonies are largely void of viable cells, with extracellular fluids and matrix fibers filling in the gaps. Another possibility is that cells deep inside the colony are dead or dormant due to the absence of nutrients, or due to other effects, such as mechanical stresses, so that the viable cells that we measure are a minority of all the bacterial cells that existed. Our experiment shows that the effect of the dead cells in a colony is negligible on the low packing density.

Furthermore, we discovered some disagreements between the experimental data and the prediction of the model. In the colonies grown for 24 hours, dead cells distribute randomly in the experiment, consistent with the prediction of the model. However, in the colonies that have passed exponential regime, we found more dead cells on the outer layers of colonies, while the model suggests the opposite. This prediction, however, is derived based on the assumption of identical physiological state of all cells, such as dead rate, cell size at birth, respiration rate. Only the growth rate of each cell is different since it depends on the concentration of local nutrients. While the size of *E. coli* newborn cells decreases as the growth rate decrease [49, 53], the cell size at death is about constant and independent of the cell size at birth [160]. We hypothesize that the cells at the center of a colony are larger at birth and spend much longer time to shrink until their size at death, and, therefore, fewer of these cells are dead towards the center of a colony.

One interpretation of the close fit between the predictions of this minimal model and the results of our soft-agar experiments is that heterogeneities beyond nutrient access contribute little to the growth dynamics of bacteria in colonies. It remains to be tested how general this result is. Is the *E. coli* in glucose-limited minimal medium used in this experiment exceptional? Will the results hold for other bacterial species and for complex media, like broth? We propose that the minimal model developed here be used as a baseline to address such question of generality with other

bacteria and media. Models are most useful when they do not fit data and thus point to other factors contributing to the studied dynamics. For growth of bacteria in colonies, such factors can be mechanical or other stresses, cell-cell interactions, and others. From an evolutionary perspective particularly intriguing in this regard would be studies of growth of bacteria in colonies initiated with multiple cells of different genotypes (or even species), where deviations from the model could signal such important phenomena as clonal competition or cooperation within a clone.

CHAPTER V

SUMMARY AND OUTLOOK

In this dissertation, three projects exploring bacterial population dynamics during infections are presented, involving both theoretical and experimental investigations. I develop a stochastic model to verify the capability of the hypothesis of independent action with phenotypic switching to explain the single−variant bottleneck in bacterial infections and interactions with the innate immune system. The minimal model employs interactions between bacteria and the immune system as well as inter-strain interactions. The failure of the optimization of the minimal model suggests that the minimal model is incapable of qualitatively explaining the single−variant bottleneck. I propose several modifications to the minimal model to fit the data well and discuss potential mechanisms of these modifications for bacterial infections in the host. These proposed modifications provide multiple directions for further investigation of this phenomenon.

To further explore the pathogenesis of bacterial infections, I designed an experimental assay with novel set-up that can be broadly applied to experimental studies of microbial population dynamics and pharmacodynamics. I applied this assay to study the efficacy of antibiotics on bacterial populations grown as colonies. This study explored the effect on the efficacy of antibiotics by various colony features, including the physical structure of bacterial colonies and the physiological states of the cells in a colony. The results of these experiments showed that the efficacy of antiobitics not only depends on the physiological states of cells in a colony, but also on the structure of the colony. As discussed in Chapter 3, the structure of a bacterial colony, instead of blocking the chemicals out of the community, affects the efficacies of antibiotics

by the intercellular interactions and the interactions between cells and the chemicals. This study provides further understanding of antibiotics treatment against bacterial infections in physically structured habitats. Hopefully, it will provoke more research on protocols of antibiotics treatment in such situations.

Last, to address the questions raised by the second project and to better understand the population dynamics of bacterial colonies, I investigate the resource-limited growth of bacterial colonies compared to plancktonic cells. In this project, I developed a coarse-grained model to describe the population dynamics with minimum heterogeneity and verify the model by conducting both population growth experiment and single-cell microscopic experiments. This study reveals similarities and differences between the populations of bacterial plancktonic cells that grow from conventional liquid cultures and of the bacterial cells in a colony. The minimal growth model developed here is capable of accounting for all observations from population dynamics experiments, provides verifiable predictions of bacterial population dynamics as colonies, while raising more questions and hypotheses of the colony structure. To verify these hypotheses, I performed single-cell experiments to image 3-d colonies incorporated with fluorescent markers using confocal microscopes. The results from this investigation agree with the predictions of the coarse-grained growth model, demonstrate quantitative features of the development of bacterial population in physically structured habitats. They should be extended to and compared to the colony studies of other bacterial species.

Bacterial populations are complex, so can be their models. However, complexity is not always better in modeling biological systems. Models are indeed very important to biological researchers. We build mathematical models based on experimental data, develop computer simulations of these models to generate predictions, and go back to experiments to verify these predictions. We can always add more complexities in a theoretical model, deriving more predictions. However, the potential of experiments

to verify these details is limited. Thus all the models developed in this dissertation were started from the minimal models and then refined to fit the available data. If a minimal model successfully explains the experimental data, as shown in Chapter 4, it indicates that adding more complexity is not necessary for the questions concerned in the current experiments. It also provides a baseline for further studies when the observations go beyond the model. On the other hand, we can still learn from a minimal model even when it fails, as shown in Chapter 2. We compare the simulated results from models to the experimental data and search for alternative solutions to fit the data better. This will require new experiments to verify those proposed assumptions. Therefore the failure of a minimal model can direct further experimental studies as well.

To summarize, in this dissertation, I present a combination of theoretical and experimental studies on bacteria infections: the within-host interactions of bacterial population and the innate immune system, the antibiotic treatment against bacterial population on physically structured habitats, and the population dynamics in 3-d colonies. I hope that these studies inspire new thoughts and stimulate further investigations towards the understanding of bacterial infections.

APPENDIX A

ANTIBIOTICS IN RICHER MEDIUM

A.1 40X MIC antibiotic exposure in 3X MHII

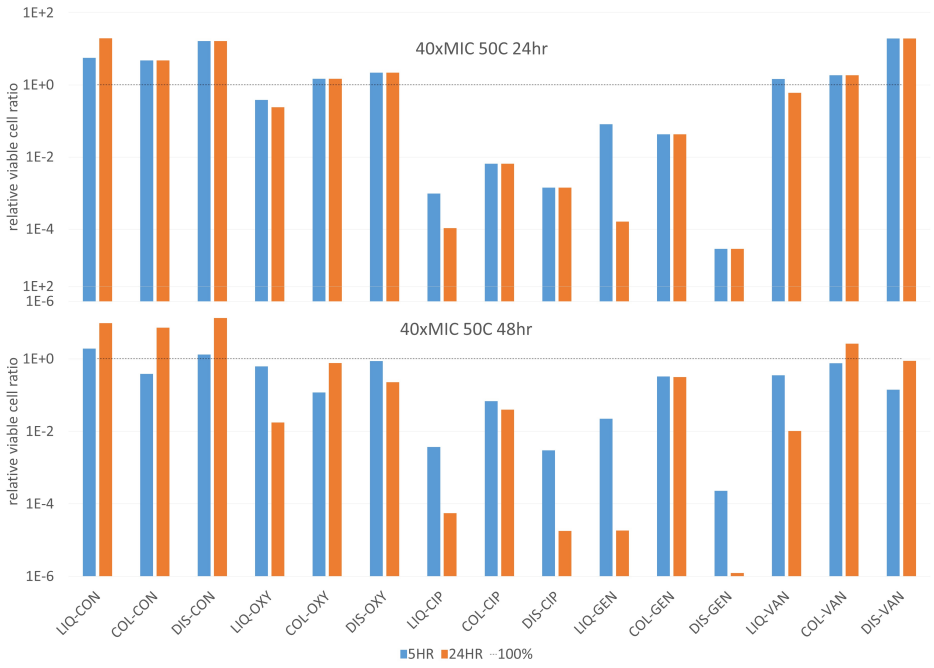

Figure A.1: The antibiotic-mediated killing of *S. aureus* Newman cultures exposed to 40X MIC of ciprofloxacin (CIP), gentamicin(GEN), vancomycin(VAN) or oxacillin (OXA) in liquid cultures(LIQ), as planktonic cells dispersed from colonies (DIS), and as intact colonies (COL). An average of 50 colonies was inoculated on each filter. The CON cultures are antibiotic-free control. Means and standard errors for three replicates. A- Cultures grown for 24 hour before exposure to the antibiotic, B- Cultures grown for 48 hours before exposure to the antibiotic. Viable cell density was measured at 5 hours after exposure (blue bars) and at 24 hours after exposure (red bars). Dashed lines represent the cell densities before transferring as a guideline.

A.2 MICs of bactericidal antibiotics in 3X MHII

In Fig. A.1, the cultures were transferred into 3X MHII liquid broth or onto 3X MHII agar with or without antibiotics. The concentrations of the bactericidal antibiotics

applied in these cultures were based on the MICs estimated in the same rich medium – 3X MHII broth. Gentamicin in 3X MHII has a 7 fold higher MIC than in standard MHII broth. The difference for the other antibiotics was not dramatic, and we used the standard MIC for those (Table.1). For the bacteria being exposed to antibiotics in 3X MHII, the concentration of gentamicin we used in this enriched-media was eventually 68 μg/ml.

Table 5: **Antibiotics' sources and MICs in 3X MHII liquid broth with different inoculum densities.** The MICs of six bactericidal antibiotics in 3X MHII broth of different concentrations and cultures initiated with different numbers of viable cells, unit of the concentrations is in μg/ml.

Antibiotics	5×10^5 **cells/ml**	5×10^7 **cells/ml**
Vancomycin	2.5	5
Gentamicin	6.9	50
Ciprofloxacin	0.6	0.6
Daptomycin	1.3	4.4
Ampicillin	1.4	2.5
Oxacillin	0.3	0.6

APPENDIX B

SUPPLEMENTAL INFORMATION ON PARAMETER FITTING OF 3-D COLONY MODEL

Table 6: **Covariances and correlations of the fitted parameters.**

$g_{\max}$, hr^{-1}	K, μg/L	a_{l}, 10^6 CFUs/μg glucose	lag, hr	m, hr^{-1}	a_{c}, hr	D, $10^6\mu\mathrm{m}^2$/hr	μ, CFUs/$\mu\mathrm{m}^3$
0.029	0.19	0.0018	0.0041	0.0047	6.0×10^4	0.018	5.1×10^4
0.99	3.4	0.022	0.047	0.23	0.11	-0.018	0.0056
0.022	*0.015*	0.0049	-0.0021	0.061	0.0023	-0.0012	1.0×10^4
0.26	*0.19*	*0.046*	0.041	-0.018	0.0035	-0.021	-2.8×10^4
0.12	*0.082*	*0.81*	*0.50*	1.8	0.070	-0.089	9.1×10^4
0.021	*0.014*	*0.23*	*0.14*	*0.28*	0.018	-0.012	4.5×10^4
0.25	*0.26*	*-0.046*	*-0.33*	*0.041*	*-0.27*	0.12	0.0033
0.19	*0.18*	*0.11*	*-0.12*	*0.24*	*0.27*	*0.77*	1.5×10^4

The upper right quadrant shows in Roman font the covariance of the fitted parameters established by bootstrapping (see *Materials and Methods*). The diagonal are the parameter variances. The lower left quadrant shows the correlation coefficients in *Italic*. Units for the parameters are the same as in Table 4. While we report these values, we emphasize that these values must be interpreted with care since posterior distributions of the parameters are sloppy [161] and do not look like multivariate normal distributions. Instead they show long nonlinear ridges of parameters with nearly-equivalent likelihoods.

REFERENCES

[1] Watts SJ. Epidemics and history: disease, power and imperialism. Yale University Press; 1999.

[2] Lee HS. Dates in Obstetrics and Gynecology: A Chronological Record of Progress in Obstetrics and Gynecology over the Last Millennium. CRC Press; 2000.

[3] Porter R. The Greatest Benefit to Mankind: A Medical History of Humanity (The Norton History of Science). WW Norton & Company; 1999.

[4] Nelson KE, Williams CFM, Masters Williams C, et al. Early history of infectious disease: epidemiology and control of infectious diseases. Infectious disease epidemiology: theory and practice. 2007;(Ed. 2):3–23.

[5] Pasteur L. The Physiological Theory of Fermentation in Scientific Papers. NY: PF Collier and Sons. 1910;.

[6] for Disease Control C, (CDC P, et al. Ten great public health achievements–United States, 1900-1999. Morb Mortal Wkly Rep. 1999;48(12):241.

[7] Ahmed R, Gray D. Immunological memory and protective immunity: understanding their relation. Science. 1996;272(5258):54.

[8] Gordon S. Elie Metchnikoff: father of natural immunity. Eur J Immunol. 2008;38(12):3257–3264.

[9] Druett H. Bacterial invasion. Nature. 1952;170(4320):288–288.

[10] Meynell G, Stocker B. Some hypotheses on the aetiology of fatal infections in partially resistant hosts and their application to mice challenged with Salmonella paratyphi-B or Salmonella typhimurium by intraperitoneal injection. Microbiology. 1957;16(1):38–58.

[11] Liu OC, Henle W. Studies on host-virus interactions in the chick embryo-influenza virus system V. Simultaneous serial passage of the agents of Influenza A and B in relation to variaations in the growth cycle of Ifluenza B virus. J Experim Med. 1951;94(4):291–304.

[12] Donald HB, Isaacs A. Counts of influenza virus particles. Microbiology. 1954;10(3):457–464.

[13] Liu OC, Henle W. Studies on host-virus interactions in the chick embryo-influenza virus system VII. Data concerning the significance of infectivity titration end-points and the separation of clones at limiting dilations. J Experim Med. 1953;97(6):889–902.

[14] Fischer W, Ganusov VV, Giorgi EE, Hraber PT, Keele BF, Leitner T, et al. Transmission of single HIV-1 genomes and dynamics of early immune escape revealed by ultra-deep sequencing. PLoS one. 2010;5(8):e12303.

[15] Bull RA, Luciani F, McElroy K, Gaudieri S, Pham ST, Chopra A, et al. Sequential bottlenecks drive viral evolution in early acute hepatitis C virus infection. PLoS Pathog. 2011;7(9):e1002243.

[16] Moxon ER, Murphy PA. Haemophilus influenzae bacteremia and meningitis resulting from survival of a single organism. Proc Natl Acad Sci (USA). 1978;75(3):1534–1536.

[17] Moxon ER, Smith A, Averill D, Smith D. Haemophilus influenzae meningitis in infant rats after intranasal inoculation. J Infect Dis. 1974;129(2):154–162.

[18] Levin BR, Antia R. Why we don't get sick: the within-host population dynamics of bacterial infections. Science. 2001;292(5519):1112–1115.

[19] Meyers LA, Levin BR, Richardson AR, Stojiljkovic I. Epidemiology, hypermutation, within–host evolution and the virulence of Neisseria meningitidis. Proc R Soc London B: Biological Sciences. 2003;270(1525):1667–1677.

[20] Margolis E, Levin BR. Within-host evolution for the invasiveness of commensal bacteria: an experimental study of bacteremias resulting from Haemophilus influenzae nasal carriage. J Infect Dis. 2007;196(7):1068–1075.

[21] Neu HC. The crisis in antibiotic resistance. Science. 1992;257(5073):1064–1073.

[22] Huycke M, Spiegel C, Gilmore M. Bacteremia caused by hemolytic, high-level gentamicin-resistant Enterococcus faecalis. Antimicrob Agents Chemother. 1991;35(8):1626–1634.

[23] Mundy L, Sahm D, Gilmore M. Relationships between enterococcal virulence and antimicrobial resistance. Clini Microbiol Rev. 2000;13(4):513–522.

[24] Costerton JW, Stewart PS, Greenberg EP. Bacterial biofilms: a common cause of persistent infections. Science. 1999;284(5418):1318–1322.

[25] Fux C, Costerton J, Stewart P, Stoodley P. Survival strategies of infectious biofilms. Trends Microbiol. 2005;13(1):34–40.

[26] Bendouah Z, Barbeau J, Hamad WA, Desrosiers M. Biofilm formation by Staphylococcus aureus and Pseudomonas aeruginosa is associated with an unfavorable evolution after surgery for chronic sinusitis and nasal polyposis. Otolaryngol Head Neck Surg. 2006;134(6):991–996.

[27] Costerton JW, Geesey G, Cheng KJ. How bacteria stick. Sci Am. 1978;238:86–95.

[28] Costerton W, Veeh R, Shirtliff M, Pasmore M, Post C, Ehrlich G. The application of biofilm science to the study and control of chronic bacterial infections. J Clin Invest. 2003;112(10):1466–1477.

[29] Post JC, Stoodley P, Hall-Stoodley L, Ehrlich GD. The role of biofilms in otolaryngologic infections. Curr Opin Otolaryngol Head Neck Surg. 2004;12(3):185–190.

[30] Sampath LA, Tambe SM, Modak SM. In vitro and in vivo efficacy of catheters impregnated with antiseptics or antibiotics: evaluation of the risk of bacterial resistance to the antimicrobials in the catheters. Infect Control Hosp Epidemiol. 2001;22(10):640–646.

[31] Antoci V, Adams CS, Parvizi J, Davidson HM, Composto RJ, Freeman TA, et al. The inhibition of Staphylococcus epidermidis biofilm formation by vancomycin-modified titanium alloy and implications for the treatment of periprosthetic infection. Biomaterials. 2008;29(35):4684–4690.

[32] Xu Y, Jones JE, Yu H, Yu Q, Christensen GD, Chen M, et al. Nanoscale plasma coating inhibits formation of Staphylococcus aureus biofilm. Antimicrob Agents Chemother. 2015;59(12):7308–7315.

[33] Wu H, Moser C, Wang HZ, Høiby N, Song ZJ. Strategies for combating bacterial biofilm infections. Int J Oral Sci. 2015;7(1):1–7.

[34] Zahller J, Stewart PS. Transmission electron microscopic study of antibiotic action on Klebsiella pneumoniae biofilm. Antimicrob Agents Chemother. 2002;46(8):2679–2683.

[35] Kreft JU, Booth G, Wimpenny JW. BacSim, a simulator for individual-based modelling of bacterial colony growth. Microbiology. 1998;144(12):3275–3287.

[36] Wimpenny JW, Colasanti R. A unifying hypothesis for the structure of microbial biofilms based on cellular automaton models. FEMS Microbiol Ecol. 1997;22(1):1–16.

[37] Picioreanu C, Van Loosdrecht MC, Heijnen JJ, et al. Mathematical modeling of biofilm structure with a hybrid differential-discrete cellular automaton approach. Biotechn Bioeng. 1998;58(1):101–116.

[38] Picioreanu C, van Loosdrecht MC, Heijnen JJ, et al. A new combined differential-discrete cellular automaton approach for biofilm modeling: application for growth in gel beads. Biotechn Bioeng. 1998;57(6):718–731.

[39] Laspidou C, Kungolos A, Samaras P. Cellular-automata and individual-based approaches for the modeling of biofilm structures: Pros and cons. Desalination. 2010;250(1):390–394.

[40] Hermanowicz SW. A model of two-dimensional biofilm morphology. Wat Sci Tech. 1998;37(4-5):219–222.

[41] Van Loosdrecht M, Heijnen J, Eberl H, Kreft J, Picioreanu C. Mathematical modelling of biofilm structures. Antoni Leeuw. 2002;81(1-4):245–256.

[42] Picioreanu C, Kreft JU, van Loosdrecht MC. Particle-based multidimensional multispecies biofilm model. Appl Environ Microbiol. 2004;70(5):3024–3040.

[43] Noguera DR, Pizarro G, Stahl DA, Rittmann BE. Simulation of multispecies biofilm development in three dimensions. Wat Sci Tech. 1999;39(7):123–130.

[44] Alpkvista E, Klapper I. A multidimensional multispecies continuum model for heterogeneous biofilm development. Bull Math Biol. 2007;69(2):765–789.

[45] Eberl HJ, Parker DF, Van Loosdrecht M. A new deterministic spatio-temporal continuum model for biofilm development. Comput Math Methods Med. 2001;3(3):161–175.

[46] Duddu R, Bordas S, Chopp D, Moran B. A combined extended finite element and level set method for biofilm growth. Int J Numer Meth Eng. 2008;74(5):848–870.

[47] Zhang T, Cogan NG, Wang Q. Phase field models for biofilms. I. Theory and one-dimensional simulations. SIAM J Appl Math. 2008;69(3):641–669.

[48] Zhang T, Cogan N, Wang Q. Phase field models for biofilms. II. 2-D numerical simulations of biofilm-flow interaction. Commun Comput Phys. 2008;4(1):72–101.

[49] Ecker RE, Schaechter M. Bacterial growth under conditions of limited nutrition. Annals NY Acad Sci. 1963;102:549–563.

[50] Koch A. Distribution of cell size in growing cultures of bacteria and the applicability of the Collins-Richmond principle. Microbiology. 1966;45(3):409–417.

[51] Kubitschek H. Growth during the bacterial cell cycle: analysis of cell size distribution. Biophysical Journal. 1969;9(6):792.

[52] Pierucci O. Dimensions of Escherichia coli at various growth rates: model for envelope growth. J Bacteriol. 1978;135(2):559–74.

[53] Taheri-Araghi S, Bradde S, Sauls JTT, Hill NSS, Levin PAA, Paulsson J, et al. Cell-Size Control and Homeostasis in Bacteria. Curr Biol. 2014;25(3):385–391.

[54] Simonsen L. Dynamics of plasmid transfer on surfaces. Microbiology. 1990;136(6):1001–1007.

[55] Pirt S. A kinetic study of the mode of growth of surface colonies of bacteria and fungi. Microbiology. 1967;47(2):181–197.

[56] Grimson MJ, Barker GC. Continuum model for the spatiotemporal growth of bacterial colonies. Phys Rev E. 1994;49.

[57] Thigpen MC, Whitney CG, Messonnier NE, Zell ER, Lynfield R, Hadler JL, et al. Bacterial meningitis in the United States, 1998–2007. N Engl J Med. 2011;364(21):2016–2025.

[58] Abel S, zur Wiesch PA, Chang HH, Davis BM, Lipsitch M, Waldor MK. Sequence tag-based analysis of microbial population dynamics. Nature methods. 2015;12(3):223–226.

[59] Kaiser P, Slack E, Grant AJ, Hardt WD, Regoes RR. Lymph node colonization dynamics after oral Salmonella typhimurium infection in mice. PLoS Pathogens. 2013;9(9):e1003532.

[60] Abel S, zur Wiesch PA, Davis BM, Waldor MK. Analysis of bottlenecks in experimental models of infection. PLoS Pathogens. 2015;11(6):e1004823.

[61] Haaland RE, Hawkins PA, Salazar-Gonzalez J, Johnson A, Tichacek A, Karita E, et al. Inflammatory genital infections mitigate a severe genetic bottleneck in heterosexual transmission of subtype A and C HIV-1. PLoS Pathog. 2009;5(1):e1000274.

[62] Wang GP, Sherrill-Mix SA, Chang KM, Quince C, Bushman FD. Hepatitis C virus transmission bottlenecks analyzed by deep sequencing. J Virol. 2010;84(12):6218–6228.

[63] Meynell G. The applicability of the hypothesis of independent action to fatal infections in mice given Salmonella typhimurium by mouth. Microbiology. 1957;16(2):396–404.

[64] Rubin LG. Bacterial colonization and infection resulting from multiplication of a single organism. Rev Infec Dis. 1987;9(3):488–493.

[65] Balaban NQ, Merrin J, Chait R, Kowalik L, Leibler S. Bacterial persistence as a phenotypic switch. Science. 2004;305(5690):1622–1625.

[66] Kussell E, Leibler S. Phenotypic diversity, population growth, and information in fluctuating environments. Science. 2005;309(5743):2075–2078.

[67] Kaufmann BB, Yang Q, Mettetal JT, van Oudenaarden A. Heritable stochastic switching revealed by single-cell genealogy. PLoS Biol. 2007;5(9):e239.

[68] Ackermann M, Stecher B, Freed NE, Songhet P, Hardt WD, Doebeli M. Self-destructive cooperation mediated by phenotypic noise. Nature. 2008;454(7207):987–990.

[69] Acar M, Mettetal JT, van Oudenaarden A. Stochastic switching as a survival strategy in fluctuating environments. Nature Genet. 2008;40(4):471–475.

[70] Elowitz MB, Levine AJ, Siggia ED, Swain PS. Stochastic gene expression in a single cell. Science. 2002;297(5584):1183–1186.

[71] Kærn M, Elston TC, Blake WJ, Collins JJ. Stochasticity in gene expression: from theories to phenotypes. Nature Rev Genet. 2005;6(6):451–464.

[72] Moxon ER, Rainey PB, Nowak MA, Lenski RE. Adaptive evolution of highly mutable loci in pathogenic bacteria. Curr Biol. 1994;4(1):24–33.

[73] Dubnau D, Losick R. Bistability in bacteria. Mol Microbiol. 2006;61(3):564–572.

[74] Davidson CJ, Surette MG. Individuality in bacteria. Annu Rev Genet. 2008;42:253–268.

[75] Jarboe LR, Beckwith D, Liao JC. Stochastic modeling of the phase-variable pap operon regulation in uropathogenic Escherichia coli. Biotechn Bioeng. 2004;88(2):189–203.

[76] O'Hanley P, Low D, Romero I, Lark D, Vosti K, Falkow S, et al. Gal-Gal binding and hemolysin phenotypes and genotypes associated with uropathogenic Escherichia coli. N Engl J Med. 1985;313(7):414–420.

[77] Peleš S, Munsky B, Khammash M. Reduction and solution of the chemical master equation using time scale separation and finite state projection. J Chem Phys. 2006;125(20):204104.

[78] Casadesús J, Low DA. Programmed heterogeneity: epigenetic mechanisms in bacteria. J Biol Chem. 2013;288(20):13929–13935.

[79] Antia R, Koella JC. A model of non-specific immunity. J Theor Biol. 1994;168(2):141–150.

[80] Artman M, Domenech E, Weiner M. Growth of Haemophilus influenzae in simulated blood cultures supplemented with hemin and NAD. J Clin Microbiol. 1983;18(2):376–379.

[81] Bancroft GJ, Bosma M, Bosma G, Unanue E. Regulation of macrophage Ia expression in mice with severe combined immunodeficiency: induction of Ia expression by a T cell-independent mechanism. J Immunol. 1986;137(1):4–9.

[82] Bancroft GJ, Schreiber R, Bosma G, Bosma M, Unanue E. AT cell-independent mechanism of macrophage activation by interferon-gamma. J Immunol. 1987;139(4):1104–1107.

[83] Barreau F, Ferrier L, Fioramonti J, Bueno L. Neonatal maternal deprivation triggers long term alterations in colonic epithelial barrier and mucosal immunity in rats. Gut. 2004;53(4):501–506.

[84] Lai YN, Yeh SL, Lin MT, Shang HF, Yeh CL, Chen WJ. Glutamine supplementation enhances mucosal immunity in rats with gut-derived sepsis. Nutrition. 2004;20(3):286–291.

[85] Lee HY, Andalibi A, Webster P, Moon SK, Teufert K, Kang SH, et al. Antimicrobial activity of innate immune molecules against Streptococcus pneumoniae, Moraxella catarrhalis and nontypeable Haemophilus influenzae. BMC Infect Dis. 2004;4(1):1.

[86] Lysenko ES, Ratner AJ, Nelson AL, Weiser JN. The role of innate immune responses in the outcome of interspecies competition for colonization of mucosal surfaces. PLoS Pathog. 2005;1(1):e1.

[87] Margolis E, Yates A, Levin BR. The ecology of nasal colonization of Streptococcus pneumoniae, Haemophilus influenzae and Staphylococcus aureus: the role of competition and interactions with host's immune response. BMC microbiology. 2010;10(1):1.

[88] Hernday A, Krabbe M, Braaten B, Low D. Self-perpetuating epigenetic pili switches in bacteria. Proc Natl Acad Sci (USA). 2002;99(suppl 4):16470–16476.

[89] Hernday AD, Braaten BA, Low DA. The mechanism by which DNA adenine methylase and PapI activate the pap epigenetic switch. Mol cell. 2003;12(4):947–957.

[90] Doan T, Mendez A, Detwiler P, Chen J, Rieke F. Multiple phosphorylation sites confer reproducibility of the rod's single-photon responses. Science. 2006;313:530–533.

[91] Cheng X, Merchan L, Tchernookov M, Nemenman I. A large number of receptors may reduce cellular response time variation. PB. 2013;10(3):035008.

[92] Waters C, Bassler B. Quorum sensing: cell-to-cell communication in bacteria. Annu Rev Cell Dev Biol. 2005;21:319–346.

[93] Fanelli D. Negative results are disappearing from most disciplines and countries. Scientometrics. 2011;90:891–904.

[94] Lees P, Cunningham F, Elliott J. Principles of pharmacodynamics and their applications in veterinary pharmacology. J Vet Pharmacol Ther. 2004;27(6):397–414.

[95] Drusano GL. Antimicrobial pharmacodynamics: critical interactions of'bug and drug'. Nature Rev Microbiol. 2004;2(4):289–300.

[96] Pankey G, Sabath L. Clinical relevance of bacteriostatic versus bactericidal mechanisms of action in the treatment of Gram-positive bacterial infections. Clin Infect Dis. 2004;38(6):864–870.

[97] Kaur P, Agarwal S, Datta S. Delineating bacteriostatic and bactericidal targets in mycobacteria using IPTG inducible antisense expression. PLoS One. 2009;4(6):e5923.

[98] French G. Bactericidal agents in the treatment of MRSA infectionsthe potential role of daptomycin. J Antimicrob Chemother. 2006;58(6):1107–1117.

[99] Monod J. The growth of bacterial cultures. Ann Rev Microbiol. 1949;3:371–394.

[100] Akins RL, Rybak MJ. In vitro activities of daptomycin, arbekacin, vancomycin, and gentamicin alone and/or in combination against glycopeptide intermediate-resistant Staphylococcus aureus in an infection model. Antimicrob Agents Chemother. 2000;44(7):1925–1929.

[101] Fuchs PC, Barry AL, Brown SD. Daptomycin susceptibility tests: interpretive criteria, quality control, and effect of calcium on in vitro tests. Diagn Microbiol Infect Dis. 2000;38(1):51–58.

[102] LaPlante KL, Rybak MJ. Impact of high-inoculum Staphylococcus aureus on the activities of nafcillin, vancomycin, linezolid, and daptomycin, alone and in combination with gentamicin, in an in vitro pharmacodynamic model. Antimicrob Agents Chemother. 2004;48(12):4665–4672.

[103] Ankomah P, Levin BR. Two-drug antimicrobial chemotherapy: a mathematical model and experiments with Mycobacterium marinum. PLoS Pathog. 2012;8(1):e1002487.

[104] Kirby AE. Synergistic action of gentamicin and bacteriophage in a continuous culture population of Staphylococcus aureus. PLoS One. 2012;7(11):e51017.

[105] Johnson PJ, Levin BR. Pharmacodynamics, population dynamics, and the evolution of persistence in Staphylococcus aureus. PLoS Genet. 2013;9(1):e1003123.

[106] Levin BR, Baquero F, Johnsen PJ. A model-guided analysis and perspective on the evolution and epidemiology of antibiotic resistance and its future. Curr Opin Microbiol. 2014;19:83–89.

[107] Ankomah P, Levin BR. Exploring the collaboration between antibiotics and the immune response in the treatment of acute, self-limiting infections. Proc Natl Acad Sci (USA). 2014;111(23):8331–8338.

[108] Knobloch JKM, Horstkotte MA, Rohde H, Mack D. Evaluation of different detection methods of biofilm formation in Staphylococcus aureus. Med Microbiol Immun. 2002;191(2):101–106.

[109] Ceri H, Olson M, Stremick C, Read R, Morck D, Buret A. The Calgary Biofilm Device: new technology for rapid determination of antibiotic susceptibilities of bacterial biofilms. J Clin Microbiol. 1999;37(6):1771–1776.

[110] Bardouniotis E, Huddleston W, Ceri H, Olson ME. Characterization of biofilm growth and biocide susceptibility testing of Mycobacterium phlei using the MBEC assay system. FEMS Microbiol Lett. 2001;203(2):263–267.

[111] Kirby AE, Garner K, Levin BR. The relative contributions of physical structure and cell density to the antibiotic susceptibility of bacteria in biofilms. Antimicrob Agents Chemother. 2012;56(6):2967–2975.

[112] Nichols WW, Evans MJ, Slack MP, Walmsley HL. The penetration of antibiotics into aggregates of mucoid and non-mucoid Pseudomonas aeruginosa. Microbiology. 1989;135(5):1291–1303.

[113] Sternberg C, Christensen BB, Johansen T, Nielsen AT, Andersen JB, Givskov M, et al. Distribution of bacterial growth activity in flow-chamber biofilms. Appl Environ Microbiol. 1999;65(9):4108–4117.

[114] Giwercman B, Jensen E, Høiby N, Kharazmi A, Costerton J. Induction of beta-lactamase production in Pseudomonas aeruginosa biofilm. Antimicrob Agents Chemother. 1991;35(5):1008–1010.

[115] Leclercq R, Cantón R, Brown DF, Giske CG, Heisig P, MacGowan AP, et al. EUCAST expert rules in antimicrobial susceptibility testing. Clin Microbiol Infect. 2013;19(2):141–160.

[116] Regoes RR, Wiuff C, Zappala RM, Garner KN, Baquero F, Levin BR. Pharmacodynamic functions: a multiparameter approach to the design of antibiotic treatment regimens. Antimicrob Agents Chemother. 2004;48(10):3670–3676.

[117] Shao X, Mugler A, Kim J, Jeong HJ, Levin B, Nemenman I. Growth of bacteria in 3-d colonies. arXiv preprint arXiv:160501098. 2016;.

[118] Udekwu KI, Parrish N, Ankomah P, Baquero F, Levin BR. Functional relationship between bacterial cell density and the efficacy of antibiotics. J Antimicrob Chemother. 2009;.

[119] Udekwu KI, Levin BR. Staphylococcus aureus in continuous culture: a tool for the rational design of antibiotic treatment protocols. PLoS one. 2012;7(7):e38866.

[120] Stewart P, Rayner J, Roe F, Rees W. Biofilm penetration and disinfection efficacy of alkaline hypochlorite and chlorosulfamates. J Appl Microbiol. 2001;91(3):525–532.

[121] Stewart PS, Davison WM, Steenbergen JN. Daptomycin rapidly penetrates a Staphylococcus epidermidis biofilm. Antimicrob Agents Chemother. 2009;53(8):3505–3507.

[122] Singh R, Ray P, Das A, Sharma M. Penetration of antibiotics through Staphylococcus aureus and Staphylococcus epidermidis biofilms. J Antimicrob Chemother. 2010;65(9):1955–1958.

[123] Siala W, Mingeot-Leclercq MP, Tulkens PM, Hallin M, Denis O, Van Bambeke F. Comparison of the antibiotic activities of daptomycin, vancomycin, and the investigational fluoroquinolone delafloxacin against biofilms from Staphylococcus aureus clinical isolates. Antimicrob Agents Chemother. 2014;58(11):6385–6397.

[124] Fuchs PC, Barry AL, Brown SD. In vitro bactericidal activity of daptomycin against staphylococci. J Antimicrob Chemother. 2002;49(3):467–470.

[125] Brauers J, Kresken M, Menke A, Orland A, Weiher H, Morrissey I. Bactericidal activity of daptomycin, vancomycin, teicoplanin and linezolid against Staphylococcus aureus, Enterococcus faecalis and Enterococcus faecium using human peak free serum drug concentrations. Int J Antimicrob Agents. 2007;29(3):322–325.

[126] Wise R, Andrews J, Ashby J. Activity of daptomycin against Gram-positive pathogens: a comparison with other agents and the determination of a tentative breakpoint. J Antimicrob Chemother. 2001;48(4):563–567.

[127] Lamp K, Rybak M, Bailey E, Kaatz G. In vitro pharmacodynamic effects of concentration, pH, and growth phase on serum bactericidal activities of daptomycin and vancomycin. Antimicrob Agents Chemother. 1992;36(12):2709–2714.

[128] Muder RR, Brennen C, Wagener MM, Vickers RM, Rihs JD, Hancock GA, et al. Methicillin-resistant staphylococcal colonization and infection in a long-term care facility. Annals of Internal Medicine. 1991;114(2):107–112.

[129] Safdar N, Andes D, Craig W. In vivo pharmacodynamic activity of daptomycin. Antimicrob Agents Chemother. 2004;48(1):63–68.

[130] Dunne W, Mason E, Kaplan SL. Diffusion of rifampin and vancomycin through a Staphylococcus epidermidis biofilm. Antimicrob Agents Chemother. 1993;37(12):2522–2526.

[131] Jefferson KK, Goldmann DA, Pier GB. Use of confocal microscopy to analyze the rate of vancomycin penetration through Staphylococcus aureus biofilms. Antimicrob Agents Chemother. 2005;49(6):2467–2473.

[132] Asally M, Kittisopikul M, Rué P, Du Y, Hu Z, Çağatay T, et al. Localized cell death focuses mechanical forces during 3D patterning in a biofilm. Proc Natl Acad Sci (USA). 2012;109(46):18891–18896.

[133] Ben-Jacob E, Schochet O, Tenenbaum A, Cohen I, Czirok A, Vicsek T, et al. Generic modelling of cooperative growth patterns in bacterial colonies. Nature. 1994;368(6466):46–49.

[134] Lobritz MA, Belenky P, Porter CB, Gutierrez A, Yang JH, Schwarz EG, et al. Antibiotic efficacy is linked to bacterial cellular respiration. Proc Natl Acad Sci (USA). 2015;112(27):8173–8180.

[135] Hunt SM, Hamilton MA, Sears JT, Harkin G, Reno J. A computer investigation of chemically mediated detachment in bacterial biofilms. Microbiology. 2003;149(5):1155–1163.

[136] Witten T, Sander L. Diffusion-Limited Aggregation, a Kinetic Critical Phenomenon. Phys Rev Lett. 1981;47:1400–1403.

[137] Ben-Jacob E, Schochet O, Tenenbaum A, Cohen I, Czirok A, Vicsek T. Generic Modeling of Cooperative Growth-Patterns in Bacterial Colonies. Nature. 1994;368:46–49.

[138] Family F. Fractal growth of bacterial colonies. Fractals. 1995;3:869–877.

[139] Lavrentovich MO, Koschwanez JH, Nelson DR. Nutrient shielding in clusters of cells. Phys Rev E. 2013;87.

[140] Levin BR. Coexistence of Two Asexual Strains on a Single Resource. Science. 1972;175(4027):1272–1274.

[141] Rojas E, Theriot JA, Huang KC. Response of Escherichia coli growth rate to osmotic shock. Proc Natl Acad Sci (USA). 2014;111(21):7807–7812.

[142] Ursell TS, Nguyen J, Monds RD, Colavin A, Billings G, Ouzounov N, et al. Rod-like bacterial shape is maintained by feedback between cell curvature and cytoskeletal localization. Proc Natl Acad Sci (USA). 2014;111(11):E1025–E1034.

[143] Bolte S, Cordelieres F. A guided tour into subcellular colocalization analysis in light microscopy. J Microsc. 2006;224(3):213–232.

[144] Efron B, Tibshirani R. An introduction to the bootstrap. Boca Raton, FL: Chapman & Hall/CRC; 1994.

[145] Marr AG, Nilson E, Clark D. The maintenance requirement of Escherichia coli. Annals NY Acad Sci. 1963;102(3):536–548.

[146] Phaiboun A, Zhang Y, Park B, Kim M. Survival Kinetics of Starving Bacteria Is Biphasic and Density-Dependent. PLoS Comp Biol. 2015 04;11(4):e1004198.

[147] Deng Y, Sun M, Shaevitz JW. Direct measurement of cell wall stress stiffening and turgor pressure in live bacterial cells. Phys Rev Lett. 2011;107(15):158101.

[148] Cayley DS, Guttman HJ, Record MT. Biophysical characterization of changes in amounts and activity of Escherichia coli cell and compartment water and turgor pressure in response to osmotic stress. Biophys J. 2000;78(4):1748–1764.

[149] Croze OA, Ferguson GP, Cates ME, Poon WC. Migration of chemotactic bacteria in soft agar: role of gel concentration. Biophys J. 2011;101(3):525–534.

[150] Kearns DB, Losick R. Swarming motility in undomesticated Bacillus subtilis. Mol Microbiol. 2003;49(3):581–590.

[151] Saint-Ruf C, Garfa-Traoré M, Collin V, Cordier C, Franceschi C, Matic I. Massive diversification in aging colonies of Escherichia coli. J Bacteriol. 2014;196(17):3059–3073.

[152] Redner S. A Guide to First-Passage Processes. Cambridge UP; 2007.

[153] Pelletier J, Halvorsen K, Ha BY, Paparcone R, Sandler SJ, Woldringh CL, et al. Physical manipulation of the Escherichia coli chromosome reveals its soft nature. Proc Natl Acad Sci (USA). 2012;109(40):E2649–E2656.

[154] Füchslin HP, Schneider C, Egli T. In glucose-limited continuous culture the minimum substrate concentration for growth, Smin, is crucial in the competition between the enterobacterium Escherichia coli and Chelatobacter heintzii, an environmentally abundant bacterium. ISME J. 2012;6(4):777–89.

[155] Chao L, Levin BR. Structured habitats and the evolution of anticompetitor toxins in bacteria. Proc Natl Acad Sci (USA). 1981;78(10):6324–6328.

[156] Buchanan R, Klawitter L. The effect of incubation temperature, initial pH, and sodium chloride on the growth kinetics of Escherichia coli O157: H7. Food Microbiology. 1992;9(3):185–196.

[157] van Stroe-Biezen SAM, Everaerts FM, Janssen LJJ, Tacken RA. Diffusion coefficients of oxygen, hydrogen peroxide and glucose in a hydrogel. Anal Chim Acta. 1993;273:553–560.

[158] Asally M, Kittisopikul M, Rue P, Du Y, Hu Z, Cagatay T, et al. Localized cell death focuses mechanical forces during 3D patterning in a biofilm. Proc Natl Acad Sci (USA). 2012;109:18891–18896.

[159] Wentland EJ, Stewart PS, Huang CT, McFeters Ga. Spatial variations in growth rate within Klebsiella pneumoniae colonies and biofilm. Biotechnol Prog. 1996;12(3):316–321.

[160] Yang J, Dungrawala H, Hua H, Manukyan A, Abraham L, Lane W, et al. Cell size and growth rate are major determinants of replicative lifespan. Cell Cycle. 2011;10(1):144–155.

[161] Gutenkunst RN, Waterfall JJ, Casey FP, Brown KS, Myers CR, Sethna JP. Universally sloppy parameter sensitivities in systems biology models. PLoS Comp Biol. 2007;3(10):1871–1878.